remote sensing

MDPI

Article

Spatial and Seasonal Variations of the Island Mass Effect at the Sub-Antarctic Prince Edward Islands Archipelago

Tarron Lamont [1,2,3,*] and Tesha Toolsee [3]

[1] Oceans & Coasts Research, Department of Forestry, Fisheries and the Environment, P.O. Box 52126, Victoria & Alfred Waterfront, Cape Town 8000, South Africa
[2] Bayworld Centre for Research & Education, 5 Riesling Road, Constantia, Cape Town 7806, South Africa
[3] Oceanography Department and Marine Research Institute, University of Cape Town, Private Bag X3, Rondebosch 7701, South Africa; tlstes001@myuct.ac.za
* Correspondence: tarron.lamont@gmail.com or tlamont@dffe.gov.za; Tel.: +27-21-819-5039

Abstract: At the sub-Antarctic Prince Edward Islands (PEIs) in the Southern Ocean, the Island Mass Effect (IME) plays an important role in maintaining an ecosystem able to support diverse biological communities; however, limited in situ sampling has severely constrained our understanding of it. As such, our study used satellite chlorophyll *a* (chla) to provide the first detailed characterisation of the spatial extent and seasonal variability of the IME at the PEIs. Seasonal surface chla variations were remarkable, with localised increases observed from mid-austral spring to the end of autumn (October to May). In contrast, during June to September, there were no distinguishable differences between chla at the PEIs and that further afield. Seasonal chla changes were significantly correlated with higher light levels, warmer waters, and shallow upper mixed layer depths reflecting enhanced water column stability during summer and autumn, with the opposite pattern in winter and spring. The IME extended northeast of the islands and remained spatially distinct from elevated chla around the northern branch of the sub-Antarctic Front and the southern branch of the Antarctic Polar Front. From December to February, the IME was spatially connected to the island shelf. In contrast, during March–May and in October, higher chla was observed only to the northeast, some distance away from the islands, suggesting a delayed IME, which has not previously been observed at the PEIs. The clear association of this higher chla with the weak mean geostrophic circulation northeast of the islands suggested retention and accumulation of nutrients and phytoplankton biomass, which was likely aided by wind-driven northeastward transport of water from the shelf. Climatological mean chla to the northeast was generally higher than that on the PEI shelf, and further research is required to determine the importance of this region to ecosystem functioning at the islands.

Keywords: Prince Edward Islands; island mass effect; satellite ocean colour; chlorophyll *a*; mixed layer depth; geostrophic currents

Citation: Lamont, T.; Toolsee, T. Spatial and Seasonal Variations of the Island Mass Effect at the Sub-Antarctic Prince Edward Islands Archipelago. *Remote Sens.* **2022**, *14*, 2140. https://doi.org/10.3390/rs14092140

Academic Editor: Cédric Jamet

Received: 21 February 2022
Accepted: 21 April 2022
Published: 29 April 2022

1. Introduction

The sub-Antarctic region of the Southern Ocean constitutes a globally important carbon sink due to the formation of intermediate, mode, and bottom waters, which sequester atmospheric CO_2 and are responsible for modulating nutrient supply and productivity at lower latitudes [1–4]. Most of the sub-Antarctic region is characterised by High Nutrient, Low Chlorophyll (HNLC) conditions, where the availability of light as well as low iron, and periodically low silicate concentrations, limits phytoplankton growth in surface waters [5–7]. A recent study [8] showed that manganese availability also played an important role in limiting macronutrient consumption and phytoplankton growth. Exceptions to HNLC conditions occur where frontal regions of the Antarctic Circumpolar Current (ACC) delimit regions of elevated chlorophyll *a* (chla) concentrations [9–11]. Similarly, around sub-Antarctic islands, localised chla enhancements (commonly referred to as the Island Mass Effect; IME), reflect phytoplankton responses to enhanced nutrient and light levels [12–15].

Located between the sub-Antarctic Front (SAF) and the Antarctic Polar Front (APF), the uninhabited Prince Edward Islands (PEIs) comprise a geologically young (~0.45 million years) archipelago [16]. Marion Island is larger, covering an area of about 270 km^2, with a peak elevation of 1230 m, while Prince Edward Island is only 45 km^2, with its highest point at 672 m above sea level [17,18]. At the PEIs, the IME (Figure 1) contributes to maintaining a diverse ecosystem that sustains rich benthic communities and large top predator populations [19–24]. Mechanisms sustaining these populations, commonly referred to as the "life-support system" of the PEIs, have been separated into inshore (autochthonous) and offshore (allochthonous) components [20,25]. While the inshore component is sustained by the IME, the offshore component is derived primarily from the advection of plankton communities toward the PEI shelf [20–22,26]. The IME is believed to be driven by the combined effects of substantial freshwater runoff from the islands, and the occurrence of a Taylor column. Freshwater runoff acts to increase nutrient availability and stratification in the surface layers, and a Taylor column structure promotes upwelling and retention of water on the shelf [27–30]. However, some studies have demonstrated that the expected localised increase in phytoplankton biomass, in response to these physical drivers, is only intermittently observed [31,32].

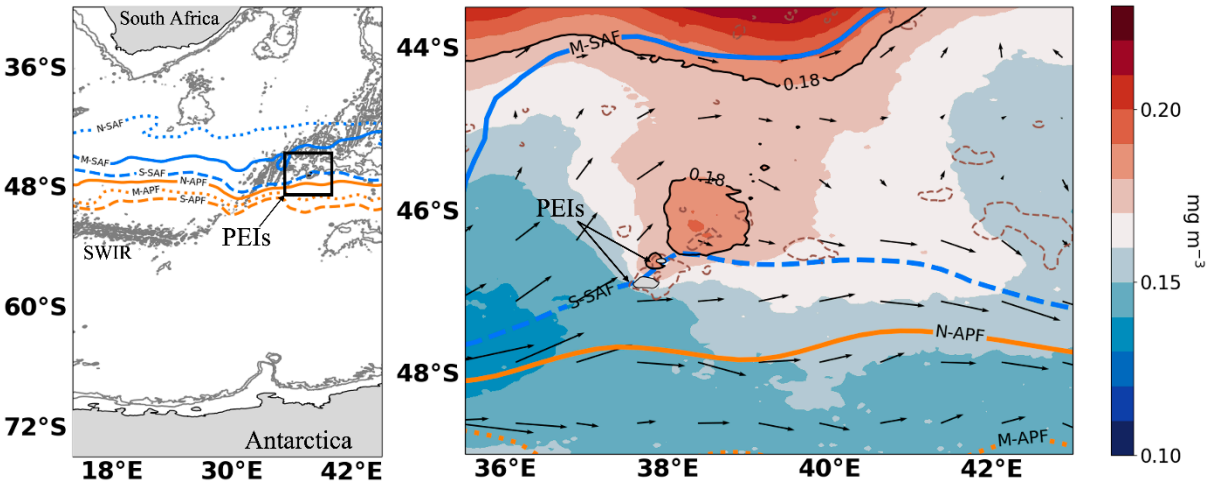

Figure 1. (**left**) Bathymetry map indicating the location of the Prince Edward Islands (PEIs) in relation to South Africa and Antarctica. The grey contours indicate the 1000, 2000, and 3000 m isobaths. (**right**) Long-term mean Copernicus-GlobColour chlorophyll *a* (chla; mg m^{-3}) in the PEI region. The black contours illustrate the 0.18 mg m^{-3} chla isopleths, and the dashed brown contours indicate the 1000 m isobath. The solid and dashed thick blue lines indicate the long-term mean positions of the middle (M-SAF) and southern (S-SAF) branches of the sub-Antarctic Front, respectively, while the solid and dotted thick orange lines show the long-term mean positions of the northern (N-APF) and middle (M-APF) branches of the Antarctic Polar Front, respectively.

Mesoscale eddies as well as meridional meanders of the SAF and APF result in highly variable oceanographic conditions at the islands, and contribute substantially to the advection of water masses and biota toward and away from the PEIs [28,31–35]. The position of the SAF relative to the PEIs is believed to be a crucial factor determining the development of phytoplankton blooms. While a more proximal location of the SAF is expected to enhance flow rates and limit retention in the inter-island region, the lower flow rates likely to occur when the SAF is further away from the islands can enhance retention and result in extensive phytoplankton blooms [25,29,36]. Earlier studies have shown a well-defined eddy corridor extending from the South-West Indian Ocean Ridge (SWIR) toward the PEIs [37–40]. However, recent investigations demonstrated that very few eddies from the SWIR get close enough to interact directly with the PEI shelf [35,41]. The vast majority of eddies influencing the islands typically form in close proximity to the islands, mainly along the southern branch of the SAF and the northern branch of the APF, and

travel on average <150 km from their origin [35,41]. There is no clear seasonal variation in the total number of eddies observed around the PEIs, or in the number of eddies directly interacting with the PEI shelf [35,41]. However, when these eddies interact with the island shelf, they can influence shelf circulation patterns for periods of a month or more, either enhancing or disrupting the flow associated with the Taylor column, depending on their orientation relative to the islands [28].

Numerous previous studies have examined the oceanographic and biological variability associated with the IME at the PEIs, e.g., [12,20,21,26,32,36,42–47]. However, their findings have been derived from limited in situ observations collected during research cruises mostly restricted to April–May each year, with very few measurements in other seasons [17], and little is known about the persistence or spatial extent of the IME at the PEIs [32,46,48]. A recent study used satellite observations and reanalysis datasets to describe the seasonal cycles of Sea Surface Temperature (SST), winds and currents around the PEIs [49]. Each year, maximum SSTs (8 °C) typically occur in February, with minimum values (5 °C) in September, but the localised cooling expected due to upwelling driven by a Taylor column is not evident in climatological mean maps. In contrast, peak wind speeds (up to 10 m s^{-1}) are usually observed in July, with minima (~7 m s^{-1}) occurring at the end of austral summer (February). Geostrophic current speeds around the islands were generally lower between April and June, with higher values during the rest of the year, particularly south of 47.5° S, while seasonal differences were less evident closer to the islands [49].

In the sub-Antarctic zone, satellite-derived surface chla data have indicated enhanced values from mid-spring to mid-summer, with generally lower values during austral autumn and winter [5,7,15,50–53]. Statistically significant long-term increases in chla have also been observed [2,54]. However, these studies mainly focused on larger spatial scales and thus do not provide a detailed view of the localised chla variability around the PEIs. Since the IME is expected to contribute substantially to sustaining a rich marine environment, it is vital to improve our understanding of its magnitude, spatial extent and variability. Thus, the present study aims to characterise the spatial and seasonal variability of the IME around the PEIs, and examine the physical factors that drive this IME variability.

2. Data and Methods

Despite the known underestimation of surface chla by satellite products in the Southern Ocean, it is commonly used as a proxy of phytoplankton biomass and primary production within the upper mixed layer [1,55]. Numerous previous studies have used satellite chla to improve the knowledge of phytoplankton variability in the Southern Ocean ([5,7,32,51–53], among others). Studies using satellite chla from a single sensor have demonstrated substantial data loss during austral autumn and winter around the PEIs, mainly as a result of limited swath width coverage and extensive cloud cover during these periods [19,51]. To overcome the limitations of single sensor products, the ocean colour community has developed multi-sensor merged and gap-free products, e.g., [56,57]. The Ocean-Colour Climate Change Initiative (OC-CCI) data is not gap-filled [57] and thus still provides limited data coverage around the PEIs, particularly during winter (Figure S1) and at shorter temporal scales. For this reason, we used the 4 km resolution multi-sensor interpolated Copernicus-GlobColour chla product, which merges data from the Sea-Viewing-Wide Field-of-View Sensor (SeaWiFS), the Medium Resolution Imaging Spectrometer (MERIS), the Moderate Resolution Imaging Spectroradiometer (MODIS) Aqua, the Visible Infrared Imaging Radiometer Suite (VIIRS-NPP), and the Ocean and Land Colour Instrument (OLCI-S3A) sensors [56]. Data between September 1997 and December 2020 were used to compute the long-term mean, standard deviation, and monthly chla climatologies, in order to investigate seasonal IME variability around the PEIs (Figures 1–3 and S2). Notably, there is good overall agreement between the spatial and seasonal variations observed from monthly climatologies of the OC-CCI data (Figure S1) and the Copernicus-GlobColour chla (Figures 1–3).

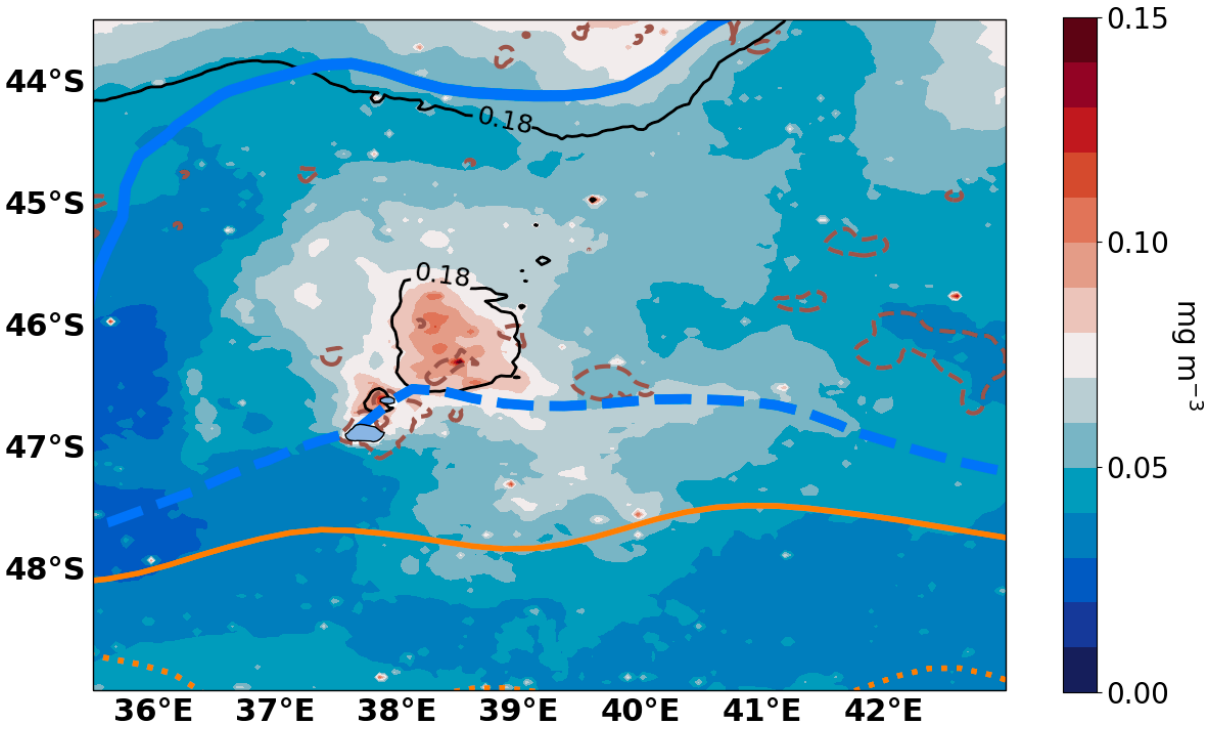

Figure 2. Standard deviation of chlorophyll *a* (chla; mg m^{-3}) in the Prince Edward Island (PEI) region. The black contours indicate the long-term mean 0.18 mg m^{-3} chla isopleths, while the dashed brown contours indicate the 1000 m isobath. The solid and dashed thick blue lines indicate the long-term mean positions of the middle (M-SAF) and southern (S-SAF) branches of the sub-Antarctic Front, respectively, while the solid and dotted thick orange lines show the long-term mean positions of the northern (N-APF) and middle (M-APF) branches of the Antarctic Polar Front, respectively.

Methods commonly used to identify the IME include the use of static contours [58], threshold values [59], the inverse relationship between chla and distance to an island [13,14], or simply examining spatially averaged data within a predefined geographical area around islands [7,60]. Given that the PEI archipelago is comprised of two unique islands and associated with a complex bathymetric structure and chla distribution (Figure 1), we have chosen to use threshold values, illustrated as static closed contours, to describe the spatial and temporal chla variations around the islands.

In order to identify and examine factors influencing the IME, chla variability was related to seasonal changes in photosynthetically available radiation (PAR), nutrients, mixed layer depth (MLD), as well as Sea Surface Temperature (SST), wind, and geostrophic currents around the PEIs. The PAR, nutrients, MLD, SST, wind, and geostrophic current products were re-gridded to match the spatial resolution of the chla in order to perform correlations per pixel across the entire study region. Monthly mean 9 km resolution PAR data from SeaWiFS between September 1997 and June 2002 [61] and MODIS-Aqua between July 2002 and December 2020 [62] were obtained from the Ocean Biology Processing Group (OBGP) at NASA's Goddard Space Flight Center (GSFC). Gridded 1° resolution monthly climatologies of surface nitrate, silicate, and phosphate, obtained from the World Ocean Atlas (WOA) 2018 [63], were used to examine the seasonality of nutrients in relation to chla variations around the PEIs. The WOA 2018 product uses all publicly available, scientifically quality-controlled in situ profile and discrete measurements to provide objectively analysed and gridded horizontal distributions of hydrographic and biogeochemical parameters across the global ocean [63].

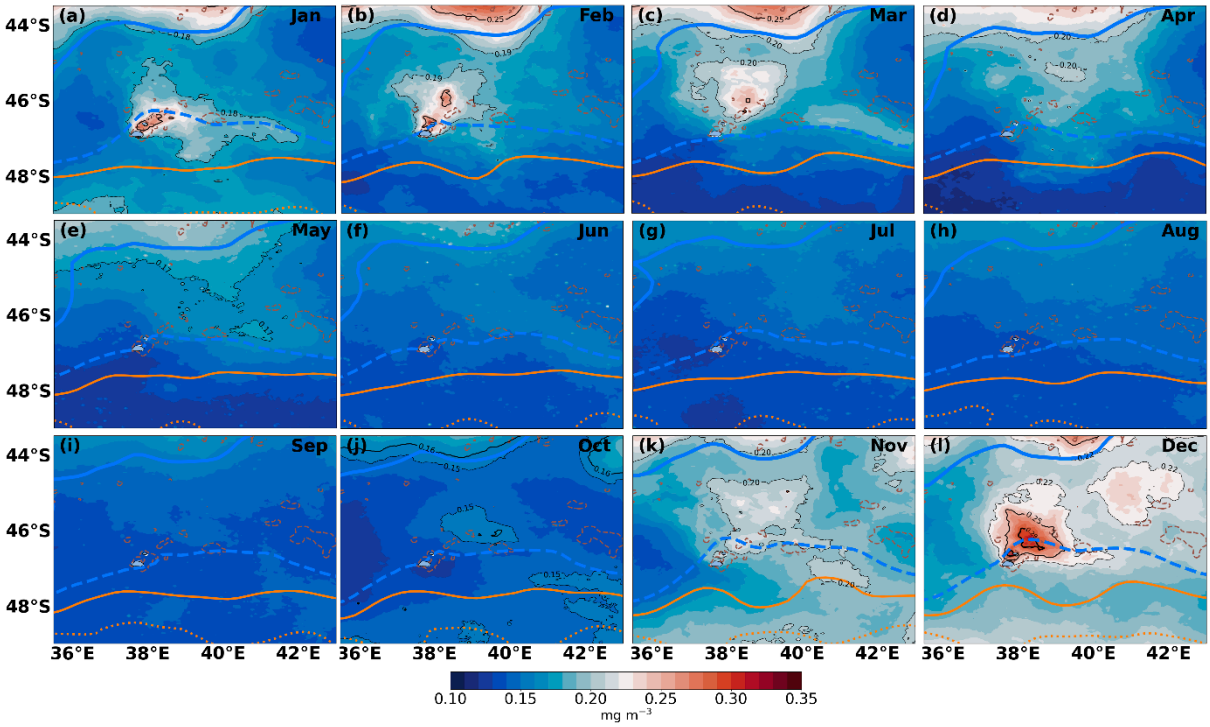

Figure 3. (**a**–**l**) Monthly (January to December) Copernicus-GlobColour chlorophyll *a* (chla; mg m^{-3}) climatology (1997–2020) in the Prince Edward Island (PEI) region. The black contours indicate the lowest and highest chla concentrations that formed unique closed contours in our region of interest (0.18 and 0.25 in January; 0.19 and 0.25 in February; 0.20 and 0.25 in March; 0.20 in April; 0.17 in May; 0.15 and 0.16 in October; 0.20 and 0.25 in November; 0.22, 0.25, and 0.29 in December). The dashed brown contours indicate the 1000 m isobath. The solid and dashed thick blue lines show the climatological mean positions of the middle (M-SAF) and southern (S-SAF) branches of the sub-Antarctic Front, respectively. The solid and dotted thick orange lines illustrate the climatological mean positions of the northern (N-APF) and middle (M-APF) branches of the Antarctic Polar Front, respectively.

The altimetry data is comprised of daily 0.25° resolution DUACS DT2018 Sea Surface Height (SSH), as well as surface geostrophic current speed and direction [64], between 1993 and 2020. This dataset is produced and distributed by the Copernicus Marine Environment Monitoring Service (CMEMS; http://marine.copernicus.eu, accessed on 25 August 2021), while the modelled surface Ekman currents [65] between 1993 and 2016 were obtained from http://globcurrent.ifremer.fr, accessed on 20 January 2021. The long-term mean positions of the northern, middle, and southern branches of the sub-Antarctic Front and the Antarctic Polar Front were identified using optimised SSH contours [28,49,66,67].

Daily 0.05° resolution SST product (1981–2020) is comprised of satellite and in situ observations optimally interpolated to produce gap-free fields [68], and was obtained from CMEMS. The ERA5 wind speeds at a pressure level of 1000 hPa, with a daily temporal resolution and 0.25° spatial resolution, over the 1979–2020 period [69], are provided by the European Center for Medium-Range Weather Forecasts (ECMWF; https://www.ecmwf.int/en/forecasts/dataset/ecmwf-reanalysis-v5, accessed on 20 January 2021). Similar to [49], wind stress was computed according to [70] and wind stress curl (WSC) was calculated following [71].

In order to identify a suitable MLD product, we qualitatively compared simulated MLD from 4 different models with a spatial resolution of 0.25°, provided by the CMEMS Global Ocean Ensemble Reanalysis product over the 1993–2019 period, with the in situ 1° resolution MLD climatology computed from Argo profiles between 2000 and 2019 [72], available at http://mixedlayer.ucsd.edu/, accessed on 25 August 2021. In terms of magnitude and spatial patterns, the monthly climatological MLD from the Ocean ReAnalysis System 5

(ORAS5) product produced by ECMWF [73] most closely matched the Argo MLD climatology (Figure S3), and thus we chose to relate the ORAS5 MLD climatology to chla variability around the PEIs. Although the remaining model reanalysis products (Figures S4–S6), viz. GLORYS2V4 [74], C-GLORS05 [75], and GLOSEA5v13 [76], compared reasonably well in terms of spatial patterns, they all showed much shallower MLD throughout the year than the ORAS5 and Argo (Figure S3) products.

3. Results

3.1. Spatial and Seasonal Chlorophyll a Patterns

The long-term mean chla (Figure 1) illustrated elevated concentrations at, as well as northeast of, the PEIs, suggesting that the enhanced chla levels in this area are a recurrent feature. In this region, the chla was 34 to 79% higher than that in the open ocean upstream of the islands (Figure 1). The recurrence of this elevated chla was further substantiated in Figure S2, which showed that for most years between 1997 and 2020, higher chla was observed during the austral spring to autumn months, albeit with considerable interannual variation in the magnitude of the chla increase. Since the present study focused on spatial and seasonal variations, more detailed analyses of the interannual chla changes will be addressed in a follow-up investigation.

Notably, the higher chla values close to the islands were distinct from the elevated concentrations around the middle branch of the sub-Antarctic Front (M-SAF) to the north of the islands (Figure 1). This is more obvious when examining chla concentrations over a larger area, as in Figure S3. Clear bands of elevated chla were centred along the northern branch of the sub-Antarctic Front (N-SAF), extending toward the M-SAF (Figure S3). Throughout the year, these bands of higher chla could be clearly distinguished from the elevated values closer to the PEIs (Figures 1 and S3). Interestingly, on the PEI shelf, the long-term mean chla illustrated that the distribution of elevated values was limited to the northern part of the PEI shelf, around the smaller Prince Edward Island, while chla across the southern portion of the shelf, around Marion Island, tended to be lower overall (Figure 1). This same pattern was evident in the monthly climatological mean chla distributions (Figure 3).

The standard deviation of the long-term mean chla (Figure 2) illustrates differences in chla variability throughout the study area. Larger standard deviations reflected greater chla variability resulting from larger seasonal and interannual changes, while smaller standard deviations indicated much lower chla variability. Regions of elevated long-term mean chla at and northeast of the PEIs (Figure 1) were associated with larger seasonal and interannual variability (Figure 2). In contrast, the surrounding open ocean regions were characterised by much lower long-term mean chla (Figure 1) with much less variability (Figure 2).

To illustrate spatial and seasonal differences, for each monthly climatological mean map (Figure 3), we highlighted both the lowest and highest chla concentrations that formed unique closed contours in our region of interest. Closed contours were identifiable from mid-austral spring to the end of autumn (October to May), in agreement with the temporal variability illustrated in Figure S3. In contrast, no closed contours were detected during winter and early spring (June to September) as there were no discernible differences between chla close to the PEIs and that in the surrounding open ocean (Figure 3). During December to February, the distribution of elevated chla was spatially connected to the island shelf. In contrast, during March–May and in October, closed contours occurred toward the northeast, some distance away from the islands. February and November were characterised by elevated concentrations both at the islands and in localised regions further northeast (Figure 3). During December, further to the northeast, a second region of enhanced chla was centred at ~45.06° S, between 40° E and 42° E (Figure 3).

The seasonal variability of surface chla around the PEIs was quite striking, with values above 0.25 mg m^{-3} only observed from December to March (Figure 3). The largest spatial extent of chla >0.25 mg m^{-3} occurred in December, and on average, values >0.29 mg m^{-3} were observed in a small area directly west of Prince Edward Island, and in a region to the northeast centred at 46.27° S; 38.31° E (Figure 3). Chla concentrations >0.25 mg m^{-3} were more spatially restricted during January–March. Values >0.18 mg m^{-3} extended to the north and further east of the PEIs in January, and appeared to be centred along the southern branch of the S-SAF. In contrast, during February, there were two distinct patches of chla >0.25 mg m^{-3} around Prince Edward Island and around 45.94° S; 38.27° E, while in March, such high values occurred only to the northeast, around 46.02° S; 38.60° E (Figure 3). During April, values exceeding 0.20 mg m^{-3} were observed in small patches northeast of the islands and in a somewhat larger area just south of 45° S, while a much smaller area of chla >0.17 mg m^{-3} occurred at about 46.44° S; 40.81° E in May. From June to September, chla at the PEIs was low and indistinguishable from the surrounding open ocean. Although chla was low overall during October, concentrations >0.15 mg m^{-3} encompassed a large area northeast of the PEIs, with the highest values (0.16 mg m^{-3}) centred around 46.06° S; 39.48° E. During November, values exceeding 0.20 mg m^{-3} showed a patchy distribution at and northeast of the PEIs. There also appeared to be an association of these patches of elevated chla with the climatological mean positions of the S-SAF and N-APF (Figure 3).

3.2. Factors Influencing Chlorophyll a Variability

3.2.1. Light, Temperature, and Nutrients

Around the PEIs, mean PAR values exceeded 25 E m^{-2} d^{-1} only from October to March, with somewhat lower values (10–25 E m^{-2} d^{-1}) occurring in April, August, and September (Figure 4). In contrast, mean PAR values during May–July were all less than 10 E m^{-2} d^{-1} (Figure 4). The seasonal chla cycle at the PEIs (Figure 3) was generally in agreement with this seasonal pattern of light availability (Figures 4 and 5a). The largest spatial extent of elevated chla in December (Figure 3) was clearly consistent with the highest light availability (Figures 4 and 5a). Statistically significant positive correlations between monthly PAR and chla around the PEIs confirmed the substantial influence of light on chla, with correlation coefficients >0.4 in a localised area around the islands, and south of 48° S (Figure 6a). However, in the region of elevated chla to the northeast of the PEIs, the mid-summer to autumn decrease in PAR preceded the decrease in chla by 2 months, with PAR decreasing from January onwards, while chla continued to increase, reaching a peak in March (Figure 5a). This suggested that a factor other than light was responsible for maintaining the elevated chla during these months. Interestingly, although light levels may be sufficient during September, there was no noticeable chla enhancement around the PEIs (Figures 3, 4 and 5a), suggesting that a different factor may be responsible for maintaining low chla in September.

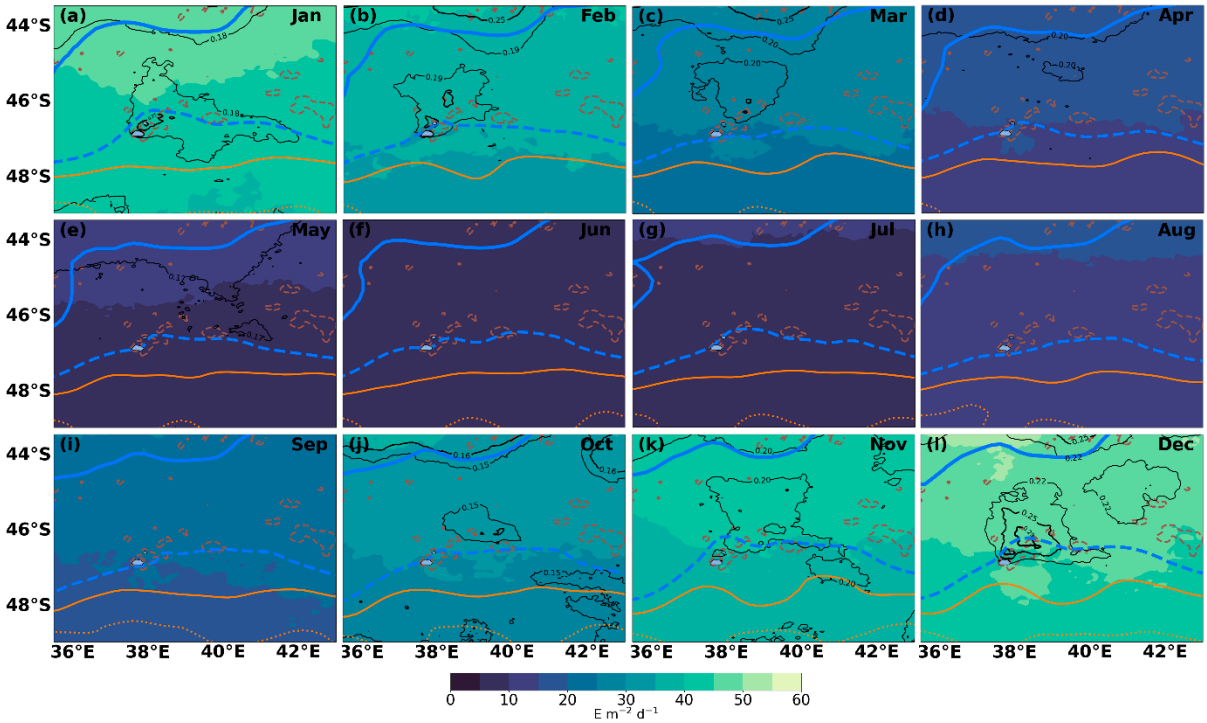

Figure 4. (**a**–**l**) Monthly (January to December) climatology (1997–2020) of SeaWiFS and MODIS Aqua Photosynthetically Available Radiation (PAR; E m^{-2} d^{-1}). The black contours indicate the lowest and highest chla (mg m^{-3}) concentrations that formed unique closed contours in our region of interest (0.18 and 0.25 in January; 0.19 and 0.25 in February; 0.20 and 0.25 in March; 0.20 in April; 0.17 in May; 0.15 and 0.16 in October; 0.20 and 0.25 in November; 0.22, 0.25, and 0.29 in December). The dashed brown contours indicate the 1000 m isobath. The solid and dashed thick blue lines show the climatological mean positions of the middle (M-SAF) and southern (S-SAF) branches of the sub-Antarctic Front, respectively. The solid and dotted thick orange lines illustrate the climatological mean positions of the northern (N-APF) and middle (M-APF) branches of the Antarctic Polar Front, respectively.

The seasonal cycles of chla and SST were generally in phase, with minima in both occurring during September in the higher chla region to the northeast of the PEIs (Figure 5b). Peak chla in December was associated with somewhat lower average SSTs, while the secondary chla peak in January and February corresponded to maximum SSTs (Figure 5b). Across most of the PEI region, the relationship between monthly SST and chla was statistically significant and positive (Figure 6b). In contrast, regions south of 48° S and east of 42° E showed no significant correlations between SST and chla, and in fact, correlations were negative in small areas east of 42° E (Figure 6b). Although the correlations with SST (Figure 6b) were generally lower than with PAR (Figure 6a), the highest values (>0.4) were once again observed in a small region on the PEI shelf and to the northeast of the islands. Stronger correlations between SST and chla were also evident around 44° S, likely associated with hydrographic variability near the M-SAF [11].

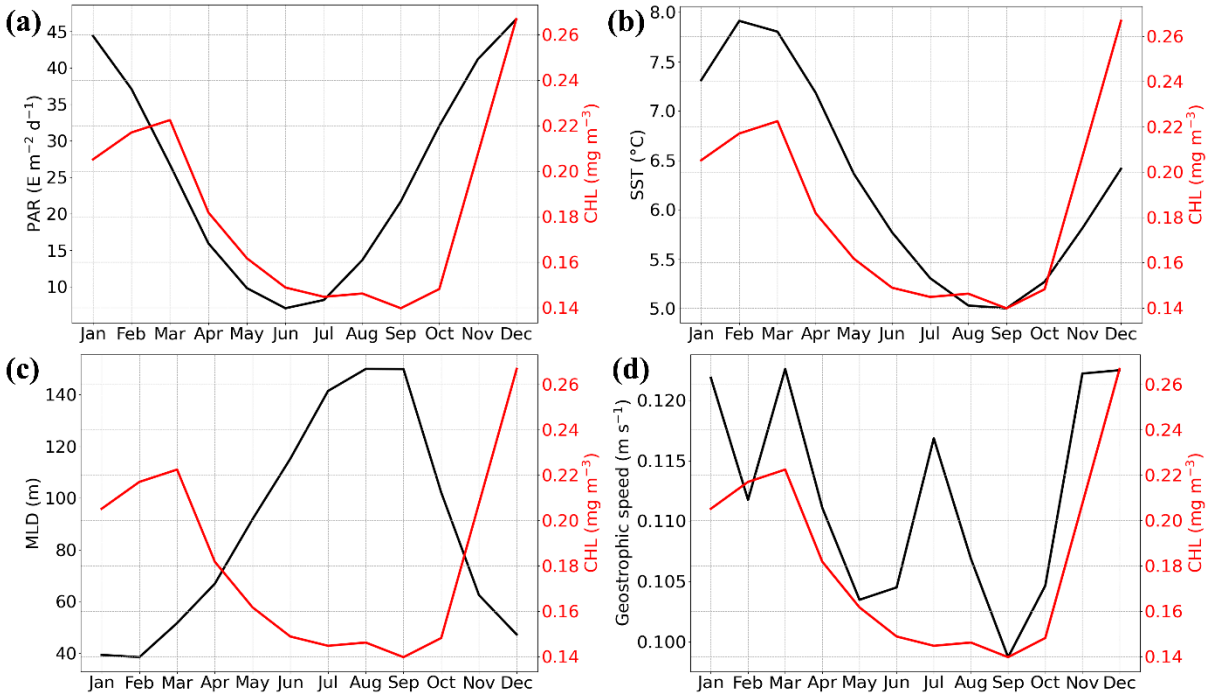

Figure 5. Monthly climatological means of chlorophyll *a* (chla; mg m^{-3}), indicated in red, and (**a**) Photosynthetically Available Radiation (PAR; E m^{-2} d^{-1}), (**b**) Sea Surface Temperature (SST, °C), (**c**) ORAS5 Mixed Layer Depth (MLD; m), and (**d**) geostrophic current speed (m s^{-1}) (shown in black), extracted and averaged over the region (45.5–46.5° S; 38–39° E) encompassed by the long-term mean 0.18 mg m^{-3} chla isopleth northeast of the Prince Edward Islands.

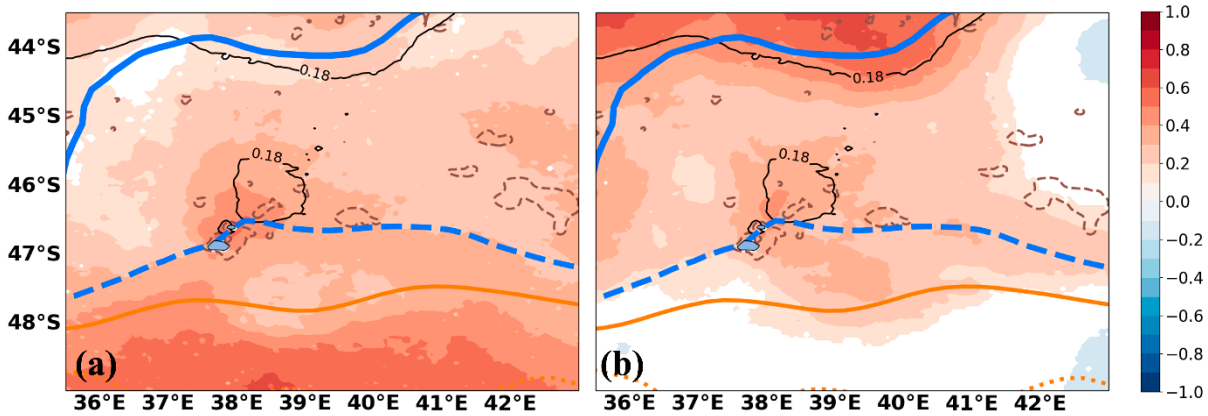

Figure 6. Pearson correlation between monthly mean chlorophyll *a* and (**a**) Photosynthetically Available Radiation, and (**b**) Sea Surface Temperature, over 1997–2020 period. The dashed brown contours show the 1000 m isobath. The black contours illustrate the long-term mean 0.18 mg m^{-3} chla isopleths. The solid and dashed thick blue lines show the long-term mean positions of the middle (M-SAF) and southern (S-SAF) branches of the sub-Antarctic Front, respectively. The solid and dotted thick orange lines illustrate the long-term mean positions of the northern (N-APF) and middle (M-APF) branches of the Antarctic Polar Front, respectively.

Since most previous studies around the PEIs have focused on describing nutrient distributions during specific autumn and summer cruises ([32,36], among others), we have examined gridded monthly climatologies of nitrate (Figure 7), silicate (Figure 8), and phosphate (Figure S8) from the WOA 2018 to better understand the seasonal nutrient changes in relation to chla variability around the PEIs. Nitrate (Figure 7), silicate (Figure 8), and phosphate (Figure S8) all showed a similar meridional gradient with lower concentrations

in the northern part of the region, and elevated values to the south of the N-APF. While nitrate concentrations remained elevated (>15 µmol kg^{-1}) throughout the year, spring and summer values were somewhat elevated compared to other seasons (Figure 7). A similar seasonal cycle was evident for silicate (Figure 8) and phosphate (Figure S8), but silicate concentrations were substantially lower (<5 µmol kg^{-1}) toward the end of summer and during autumn. Correlations between nutrients and chla were weak and statistically insignificant (not shown), likely due to the coarse spatial resolution of the nutrient observations.

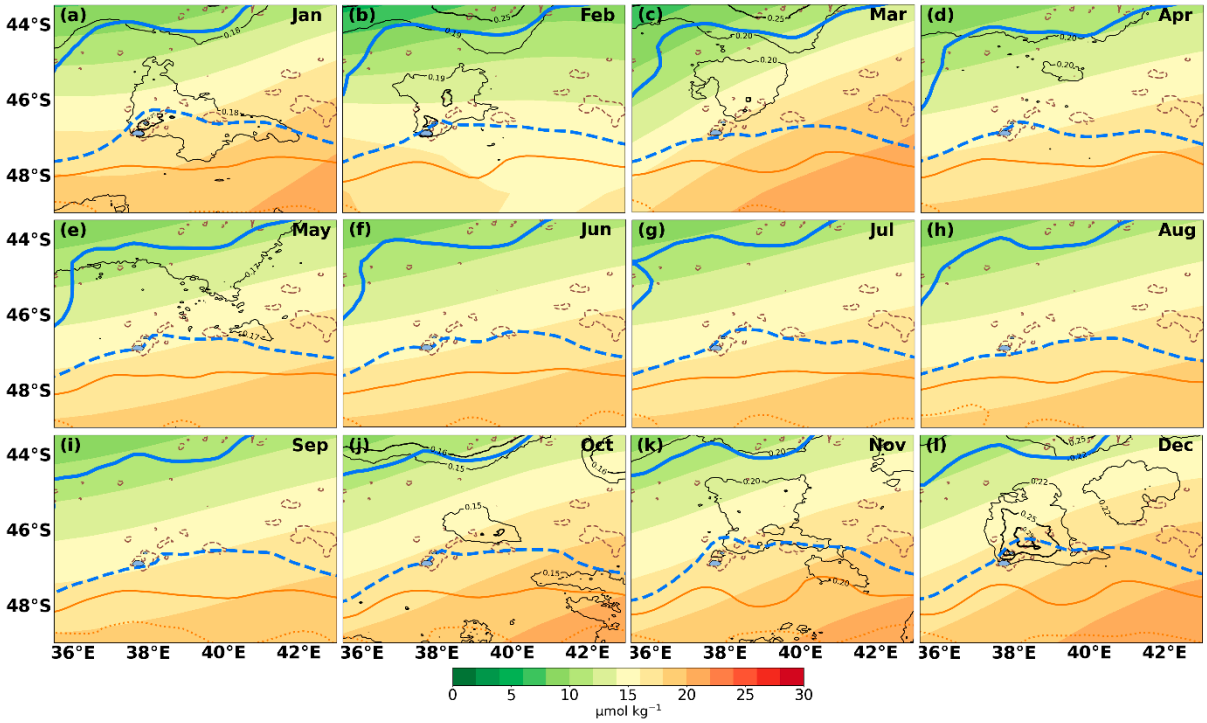

Figure 7. (**a**–**l**) Monthly (January to December) World Ocean Atlas 2018 climatology of nitrate (µmol kg^{-1}). The black contours indicate the lowest and highest chla (mg m^{-3}) concentrations that formed unique closed contours in our region of interest (0.18 and 0.25 in January; 0.19 and 0.25 in February; 0.20 and 0.25 in March; 0.20 in April; 0.17 in May; 0.15 and 0.16 in October; 0.20 and 0.25 in November; 0.22, 0.25, and 0.29 in December). The dashed brown contours indicate the 1000 m isobath. The solid and dashed thick blue lines show the climatological mean positions of the middle (M-SAF) and southern (S-SAF) branches of the sub-Antarctic Front, respectively. The solid and dotted thick orange lines illustrate the climatological mean positions of the northern (N-APF) and middle (M-APF) branches of the Antarctic Polar Front, respectively.

3.2.2. Mixed Layer Depths, Winds, and Currents

In the PEI region, shallower MLD (23–84 m) occurred during late spring (November) to mid-autumn (April), and appreciably deeper MLD (49–200 m) was observed from May to October (Figure 9). Notably, from June to October, some of the deepest MLDs were located close to the PEIs (Figure 9). As expected, the seasonal cycles of chla and MLD were out of phase, with maximum MLD corresponding to minimum chla, and vice versa (Figure 5c). Statistically significant negative correlations were observed across most of the region, with the strongest correlations (<−0.4) extending northeast from the PEI shelf (Figure 10). Similarly strong correlations were also observed north of 44° S (Figure 10). Although light levels may be sufficient for phytoplankton growth in September (Figures 4 and 5a), MLDs are still relatively deep, ranging between 79 and 198 m (Figures 5c and 9), possibly accounting for the lack of substantial chla increase during this month (Figures 3 and 5c), at least on a climatological scale. Interestingly, chla started increasing in October when MLDs were still relatively deep

(49–133 m) (Figures 3, 5c and 9). This has also been observed at the Crozet, Kerguelen, and the South Georgia Islands [15,52,77,78].

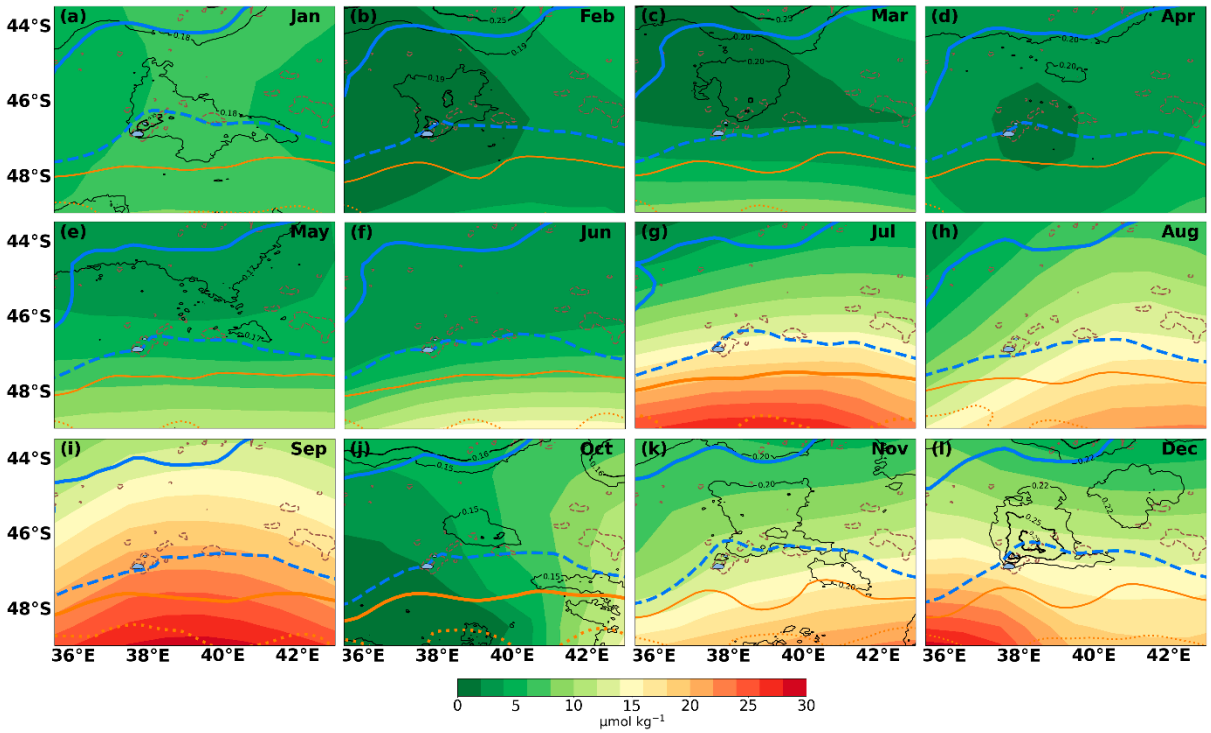

Figure 8. (**a**–**l**) Monthly (January to December) World Ocean Atlas 2018 climatology of silicate (µmol kg^{-1}). The black contours indicate the lowest and highest chla (mg m^{-3}) concentrations that formed unique closed contours in our region of interest (0.18 and 0.25 in January; 0.19 and 0.25 in February; 0.20 and 0.25 in March; 0.20 in April; 0.17 in May; 0.15 and 0.16 in October; 0.20 and 0.25 in November; 0.22, 0.25, and 0.29 in December). The dashed brown contours indicate the 1000 m isobath. The solid and dashed thick blue lines show the climatological mean positions of the middle (M-SAF) and southern (S-SAF) branches of the sub-Antarctic Front, respectively. The solid and dotted thick orange lines illustrate the climatological mean positions of the northern (N-APF) and middle (M-APF) branches of the Antarctic Polar Front, respectively.

In the PEI region, wind speeds tend to be greater during winter, with overall weaker winds during summer [49,79], opposite to the seasonal chla variability (Figure 3). Across most of our study area, the relationship between wind speed and chla was not statistically significant (Figure S9a). Negative wind stress curl induces divergence at the surface that enhances the uplift of nutrients and can stimulate phytoplankton growth. In the PEI region, negative wind stress curl occurs throughout the year, with localised enhancement over the islands and toward the east [49]. Although patchily distributed and generally weak (<0.3), statistically significant positive correlations between wind stress curl and chla east of the PEIs (Figure S9b) suggest that at least some of chla enhancement in this region can be attributed to the effects of wind stress curl. Notably, a small region of positive wind stress curl, which occurs directly southeast of the PEIs throughout the year [49], would promote downwelling conditions. This likely contributes to the maintenance of deep MLDs east of the islands, particularly between July and September (Figure 9). The generally west-northwesterly winds in the PEI region result in surface Ekman currents and transport directed toward the northeast [49]. As such, even though correlations between Ekman currents and chla were weak (<0.1) and patchily distributed (Figure S9d), wind speed and stress variations are expected to play some role in transporting surface waters from the PEI shelf toward the northeast, contributing to the enhanced chla northeast of the islands (Figures 1 and 3).

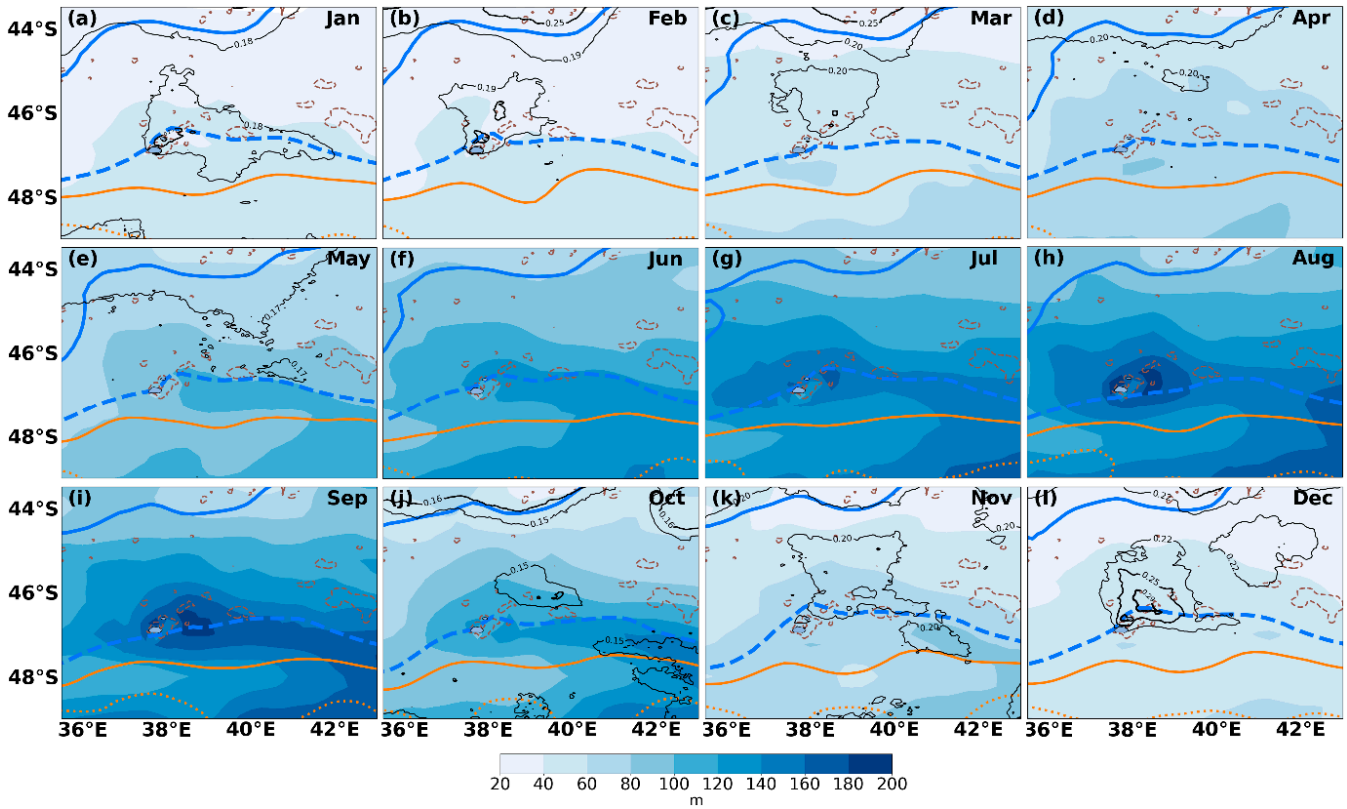

Figure 9. (**a**–**l**) Monthly (January to December) climatology (1993–2019) of the ORAS5 simulated mixed layer depth (m). The black contours indicate the lowest and highest chla (mg m^{-3}) concentrations that formed unique closed contours in our region of interest (0.18 and 0.25 in January, 0.19 and 0.25 in February, 0.20 and 0.25 in March, 0.20 in April, 0.17 in May, 0.15 and 0.16 in October, 0.20 and 0.25 in November, 0.22, 0.25, and 0.29 in December). The dashed brown contours indicate the 1000 m isobath. The solid and dashed thick blue lines show the climatological mean positions of the middle (M-SAF) and southern (S-SAF) branches of the sub-Antarctic Front, respectively. The solid and dotted thick orange lines illustrate the climatological mean positions of the northern (N-APF) and middle (M-APF) branches of the Antarctic Polar Front, respectively.

The climatological mean geostrophic currents (Figure 11) illustrated bifurcation of the ACC flow around the PEIs, resulting in the formation of a region of relatively weak currents in the lee of the islands, in agreement with previous studies [40,43,49]. From October to May, areas of enhanced chla (Figure 3) corresponded closely to areas of generally lower current speeds (Figure 11), suggesting possible retention and accumulation of nutrients and phytoplankton biomass in these regions. However, the mean seasonal cycles of chla and geostrophic current speed in Figure 5d showed that they were generally in phase, with elevated chla during summer and autumn corresponding to peaks in geostrophic current flow. Thus, at least some of the chla response in this region likely results from advection by the prevailing currents, with periods of stronger advection associated with higher chla concentrations. In the elevated biomass region to the northeast of the PEIs, correlations between chla and geostrophic currents were weak and statistically insignificant, but closer to the M-SAF and M-APF, areas of weak to moderate (0.2 to 0.3) positive correlations (Figure S9c) agreed with the seasonal cycles in Figure 5d, and with observations from previous studies [9–11]. Closer to the PEIs, these correlations were negative, weak (smaller than −0.2), and statistically significant only in small localised areas (Figure S9c), suggesting that increased current speeds may cause some reduction of surface chla especially upstream of the islands, likely through increased turbulence and stronger advection of surface waters away from the PEI shelf.

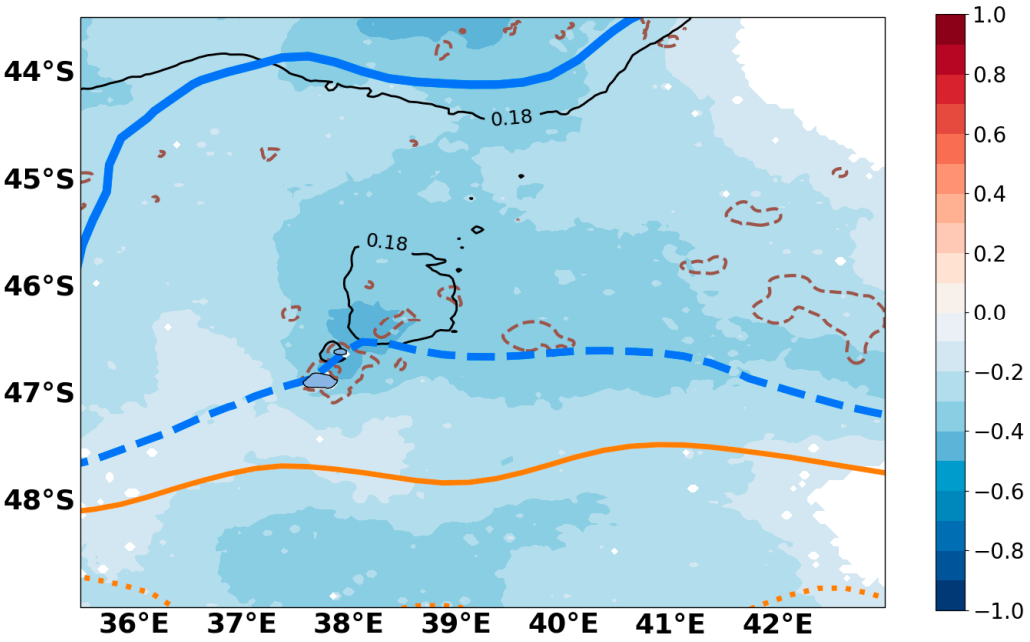

Figure 10. Pearson correlation between monthly mean chlorophyll *a* and ORAS5 simulated mixed layer depth over the 1997–2020 period. The dashed brown contours show the 1000 m isobath. The black contours illustrate the long-term mean 0.18 mg m^{-3} chla isopleths. The solid and dashed thick blue lines show the climatological mean positions of the middle (M-SAF) and southern (S-SAF) branches of the sub-Antarctic Front, respectively. The solid and dotted thick orange lines illustrate the climatological mean positions of the northern (N-APF) and middle (M-APF) branches of the Antarctic Polar Front, respectively.

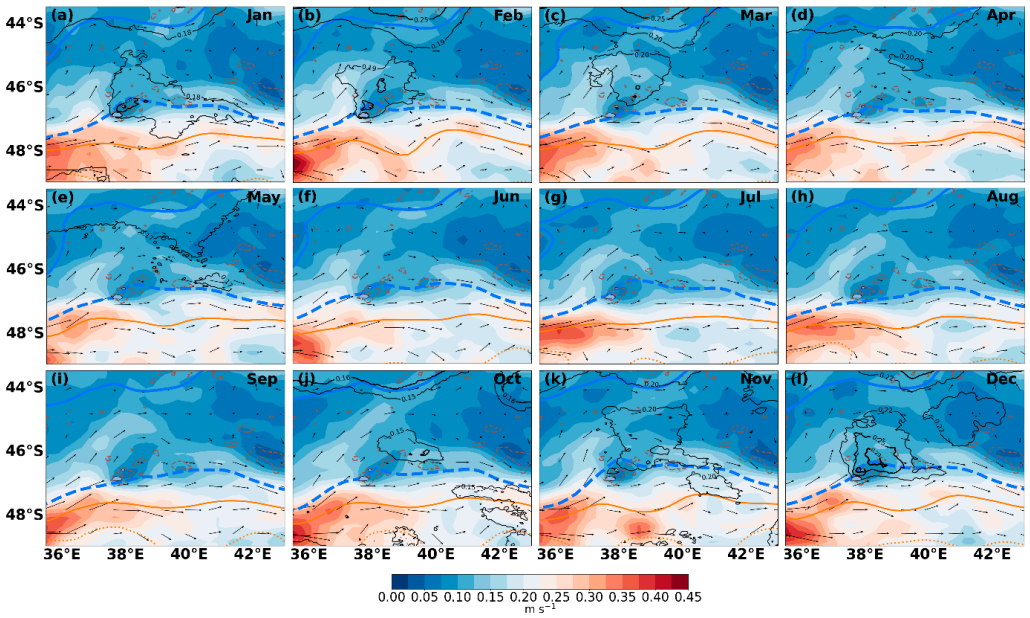

Figure 11. (**a**–**l**) Monthly (January to December) climatology (1993–2020) of geostrophic current speed (m s^{-1}). The vectors indicate the direction of current flow, while the black contours indicate the lowest and highest chla (mg m^{-3}) concentrations that formed unique closed contours in our region of interest for each month (0.18 and 0.25 in January; 0.19 and 0.25 in February; 0.20 and 0.25 in March; 0.20 in April; 0.17 in May; 0.15 and 0.16 in October; 0.20 and 0.25 in November; 0.22, 0.25, and 0.29 in December). The dashed brown contours indicate the 1000 m isobath. The solid and dashed thick blue lines show the climatological mean positions of the middle (M-SAF) and southern (S-SAF) branches of the sub-Antarctic Front, respectively. The solid and dotted orange lines illustrate the climatological mean positions of the northern (N-APF) and middle (M-APF) branches of the Antarctic Polar Front, respectively.

4. Discussion

Numerous previous studies [50–54] have examined seasonal and interannual chla variability at larger spatial scales across the Southern Ocean. However, their focus on basin and larger scales and zonally averaged patterns has not necessarily provided a clear depiction of the variability at more regional and local scales around the PEIs [3,80]. Despite many earlier in situ studies of phytoplankton variability at and around the PEIs, there is still little knowledge on the seasonality of these patterns due to constrained sampling [17,26,32,46,47]. To our knowledge, the present study provides the first detailed satellite-based investigation of spatial and seasonal chla variations around the PEIs, thus improving the knowledge of local chla variability around the islands.

4.1. Chlorophyll a Variability

To the north and south of the PEIs, the elevated chla around the middle branches of the sub-Antarctic Front and the Antarctic Polar Front (Figures 3 and S3) during summer and autumn agreed well with previous larger scale investigations [2,9–11]. Similarly, the localised chla increase at the PEIs from mid-austral spring to the end of autumn (Figures 1, 3 and S3) also agreed with previous studies that have observed the IME around island ecosystems. In the Pacific Ocean, [13] showed that the IME increased chla by up to 85.6% over background conditions around islands and at atolls. In the Southern Ocean, individual phytoplankton blooms around the Kerguelen, Crozet, and South Georgia Islands have often been associated with chla >2 mg m^{-3} [7,15,77,81,82]. At the Kerguelen plateau, the IME occurs only during austral spring and summer, with the largest areal extent observed in December downstream of the northern part of the plateau, and over the southern part in January [59]. In shallow waters (<1000 m) between the Kerguelen and Heard Islands, phytoplankton blooms start in November, while those to the north (40–45° S) start in January [52]. North of the Crozet Plateau, phytoplankton bloomed annually from September to January [78]. At South Georgia, phytoplankton blooms occur between October and March [15,77,82].

Previous in situ chla measurements on the PEI shelf range between 0.01 and 2.8 mg m^{-3}, with only a few studies documenting values above 1 mg m^{-3} [26,32,46]. The phytoplankton blooms at the PEIs, as well as Bouvet and Macquarie Islands, do not seem to be as large as those at the Kerguelen, Crozet, and South Georgia Islands [7]. Similarly, [46] showed that phytoplankton biomass at the PEIs was generally much lower and more spatially restricted than those at the Crozet and Kerguelen Islands. These differences among sub-Antarctic islands may be due to variations in shelf area or sediment characteristics which cause disparities in the iron flux exported to the surrounding surface waters [10,78,83]. More recently, [13] showed that island ecosystems with larger shelf areas in the Pacific Ocean are associated with a more marked IME. Previously, [7] noted that, in comparison to Kerguelen (7215 km^2), Crozet (352 km^2), and South Georgia (3756 km^2), the smaller PEIs (with Marion being 270 km^2 and Prince Edward 45 km^2) and Macquarie (128 km^2) systems have a much weaker impact on surrounding current flows. In addition, these systems are not associated with large shallow shelf areas where iron can accumulate in the surface waters during winter.

The extension of elevated chla values northeast of the PEIs is particularly noteworthy since no previous studies have documented such a recurrent chla pattern associated with the islands. This is not surprising, given that most previous in situ sampling did not extend that far northeast of the islands [17,26,46,47]. It is well known that biological responses associated with IME processes are not always confined to the immediate vicinity of islands. Increased phytoplankton biomass often extends over large areas downstream of islands due to passive advection by prevailing currents, and because of isopycnal shoaling within eddies formed in the lee of islands [58,84–86]. Elevated phytoplankton biomass levels have also been associated with mesoscale eddies around the PEIs [31,33,34]. A recent study [32] examined gridded surface chla patterns to contextualise in situ chla variations observed during summer and autumn cruises. At daily timescales during the cruise periods,

surface chla values on the PEI shelf were also generally lower, with elevated concentrations observed further offshore, especially northeast of the islands [32], in agreement with the mean spatial patterns described in this study. While upwelling and advection by mesoscale eddies likely drove some of the chla response northeast of the PEIs, such eddies were not always present when chla was elevated [32].

A recent study [86] distinguished between "classical IMEs", characterised by elevated chla that remains spatially connected to islands, and "delayed IMEs", during which phytoplankton respond so slowly to enhanced light and nutrient conditions that the bloom becomes separated from islands as water masses are advected further afield. On a climatological scale, both of these definitions seem to apply to the chla distributions around the PEIs. During December to February, the distribution of elevated chla was spatially connected to the island shelf, suggesting the existence of a classical IME at the PEIs. In contrast, during March–May, and in October, closed contours occurred toward the northeast, some distance away from the islands, suggesting a possible delayed IME. February and November were characterised by elevated concentrations both at the islands, and in localised regions further northeast, suggesting the occurrence of both classical and delayed IMEs during these months (Figure 3). However, more detailed in situ sampling or high spatial and temporal resolution modelling experiments will be required to confirm our hypothesis of a delayed IME at the PEIs.

4.2. Influence of Environmental Forcing on Chlorophyll a Variations

Seasonal variations in Southern Ocean phytoplankton biomass are strongly controlled by the seasonality of incoming solar irradiance, which determines light availability and influences water column stability and hence nutrient (especially iron, silicate, and manganese) supply to the euphotic zone [5,8,9,87,88]. In the sub-Antarctic zone, light availability at the surface is sufficient for stimulating phytoplankton growth from September to April [7,50], with the highest light levels observed in December and January [89,90]. This same pattern was observed more locally around the PEIs (Figures 4, 5a and 6a).

Temperature exhibits substantial control on phytoplankton biomass and production. While generally inverse relationships have been observed between temperature and phytoplankton biomass at global scales [91–94], more regionally-focused analyses have described positive and even non-linear relationships, e.g., [95–97]. In the Southern Ocean, [98] demonstrated increased phytoplankton growth in response to elevated temperatures, and a recent study by [99] also showed substantial increases in chla concentrations associated with elevated temperatures during marine heatwave conditions in the sub-Antarctic region. At a seasonal scale around the PEIs, the positive correlations between SST and chla reflect the known seasonal variability, where elevated chla is observed during the austral spring to autumn months (Figures 3, S3 and 5b), when surface waters are generally warmer, ranging between 5.5 and 8 °C [49].

Large-scale variability of nutrients around the PEIs is mainly controlled by meridional movements of the ACC fronts, and by advection of Antarctic and sub-Antarctic Surface Waters from mesoscale eddies [32,36,100]. Gridded nutrient distributions (Figures 7, 8 and S8) agreed well with previous larger-scale descriptions [1] and more regionally focused studies around other sub-Antarctic islands, e.g., [101,102]. However, due to their coarse spatial resolution, they do not reflect the smaller scale spatial variations and localised nutrient enhancement described around the PEIs by previous studies. Limited observations during summer and autumn cruises between 2008 and 2018 have also not been able to capture such nutrient enhancement [32].

Freshwater runoff from the islands introduces nutrients (particularly ammonia, urea, and phosphate) to shelf waters (up to 80 km offshore), promoting increased water column stability and periodic phytoplankton blooms [20,21,29,30]. Maximum phosphate concentrations, derived from the mineralization of feathers, tend to occur in April and May in shallow shelf waters [20,21]. A recent investigation by [103] showed that on the PEI shelf, $\delta^{13}C$ of surface suspended particulate matter (SPM) during April–May of 2015 to 2017

reflected phytoplankton as a source of SPM, while $\delta^{15}N$ values suggested enhanced nutrient recycling and smaller phytoplankton species during autumn. Similarly, [46] observed small ratios of new to total production, suggesting that phytoplankton growth during April–May 2017 was driven mainly by regenerated nutrients. Peak guano production (associated with the introduction of ammonia and urea in shallow waters) occurs from December to February [20,21]. This coincides with peak rainfall during December and January [79], and with the strongest IME (Figures 3, 5 and S3).

Throughout the open ocean regions in the Southern Ocean, previous studies, e.g., [8] have demonstrated widespread manganese limitation, or iron-manganese co-limitation. To our knowledge, there have not been any investigations of iron or manganese concentrations close to the PEIs, but it is likely that the PEI shelf sediments serve as a source of iron to surrounding surface waters, as observed for other sub-Antarctic islands [7,9,52,77,87]. Recent studies have suggested that dissolved iron and carbon availability for phytoplankton populations in the Southern Ocean may be affected by interactions between autotrophic and heterotrophic microbes [90,104], but to date, there is no clear understanding of such interactions at the PEIs. Nevertheless, the large spatial extent and recurrence of elevated chla around the PEIs from mid-spring to mid-autumn (Figures 1, 3, 5, S2 and S3) is consistent with an environment where nutrients within the surface layers are not limiting (Figures 7, 8 and S8). This also agrees with photophysiological measurements at the PEIs during December 2008, which suggested that the phytoplankton community was not limited by iron or nitrate, but may have been somewhat constrained by substantially low silicate values [36]. However, observations of low ratios of new to total production, as well as regenerated nitrogen uptake rates, and the dominance of smaller phytoplankton, suggested some iron limitation in April–May 2017 [46,103]. The findings from these previous studies also suggest that a considerable proportion of the primary production at the PEIs, at least during autumn, may be driven by regenerated nutrients as opposed to new production driven by nitrate inputs, but more detailed investigations will be required to determine this with accuracy.

When nutrients are not limiting, chla increases are strongly correlated with MLD variations [7,53]. Across the Southern Ocean, surface MLDs are typically much shallower (<100 m) and less variable during summer. In contrast, winter surface MLDs extend much deeper (up to 600 m in some locations) and exhibit considerably more spatial variation [7,53,72]. A similar seasonal pattern occurred locally around the PEIs (Figure 9). Shoaling of the MLD during summer provides irradiance conditions favouring phytoplankton growth, while deeper MLD in winter results in the dilution of phytoplankton communities over a larger depth range and further reduces the light to which phytoplankton are exposed (Figures 5c and 10) [7,53]. The deep mixing and associated strong turbulence during winter months has also been observed on the shallow inter-island shelf [28], and likely allows for the water column replenishment of dissolved iron and other micronutrients from surface sediments [50,78,102,105]. Previous studies at the PEIs have also shown that water column stability accounts for a substantial proportion of the variability in phytoplankton biomass and primary production on the shelf [29,30,36,46].

MLDs are either strengthened or eroded by the combined effects of turbulent mixing (driven by wind stress variations) and buoyancy forcing (driven by advection, entrainment, fresh water input, and air-sea exchange). Across most of the global ocean, higher wind speeds are generally associated with elevated surface chla, since stronger wind mixing allows entrainment of more nutrients into the surface layers and can also mix subsurface chla maxima up to the surface [94]. In the Southern Ocean, negative correlations between wind speed and chla have been observed [106,107]. While stronger/weaker wind speeds during winter/summer at the PEIs [49,79] were associated with lower/higher chla (Figures 3 and S3), correlations were weak and statistically insignificant (Figure 9a), in agreement with [106]. Nevertheless, wind speed and stress variations are expected to contribute to the advection of shelf waters from the PEI shelf to the northeast. A recent study at the Kerguelen Plateau [108] also demonstrated the importance of wind stress variations in controlling turbulence and the

depth of the actively mixing layer, and consequently chla. They illustrated rapid shallowing of the mixed layer from 250 m to 70–80 m over a 10-day period at the end of October 2016, with concomitant chla increases from 0.5 to 2.5 mg m^{-3} [108]. Large event-scale increases in silicate concentrations on the Kerguelen Plateau following a storm have also been described [109]. Such substantial event-scale variability likely also exists at the PEIs, but is smeared by the use of monthly means, and its examination is beyond the scope of the present study.

To the north and south of the PEIs, the elevated chla around the SAF and APF (Figures 3 and S3) reflected the phytoplankton response to enhanced advection and stronger vertical exchange of nutrients and biota along the frontal regions. As described earlier, there was also a clear eastward extension of elevated chla along the S-SAF during these months (Figures 3 and 11), suggesting the advection of higher chla waters away from the island shelf. This has also been reported by previous studies, particularly downstream of areas where the fronts interact with bathymetric features [9–11]. Previous studies have suggested that the position of the SAF relative to the PEIs plays an important role in controlling the development of phytoplankton blooms on the shelf [25,29,36]. Changes in the diversity and structure of phytoplankton and bacterial communities have also been associated with the S-SAF [47]. Recently, [49] showed that seasonal variation in the position of the S-SAF was relatively weak, being located closest to the PEIs in winter, and only slightly further north during summer. This same pattern was evident in our study (Figures 3 and 11). The slightly more northerly location of the S-SAF during November to January coincides with the strongest IME (Figures 3 and 11), suggesting that flow rates may be somewhat lower, resulting in increased retention during these months, in agreement with previous hypotheses [29,36]. However, the altimetry data (Figure 11) does not clearly indicate these lower flow rates during spring and summer, likely due to their coarse spatial resolution, and thus additional studies are required to determine the influence of the S-SAF on flow rates, retention, and chla on the PEI shelf.

The region of elevated chla northeast of the PEIs was associated with weak mean circulation (Figure 11), suggesting that the bifurcation of ACC flow around the PEIs contributes to retention and accumulation of nutrients and phytoplankton biomass in the lee of the islands. Similarly, it has been shown that the extremely weak mean circulation to the north of Crozet allows dissolved iron from the island shelf to accumulate during winter months [102,105], stimulating substantial phytoplankton blooms during subsequent summer months when light levels and stratification become conducive [78].

Stronger eastward geostrophic currents were associated with the flow of the ACC upstream and south of the islands throughout the year (Figure 11). This flow pattern has also previously been demonstrated [49]. It is likely that this consistently strong flow maintains the lower chla concentrations south of Marion Island through persistent advection of high chla waters away from the island (Figures 1 and 3). In contrast, the northward deflection of current flow upstream of the islands results in comparatively weaker current speeds (Figure 11) on the somewhat wider shelf to the west of Prince Edward Island (Figure 1), allowing for the retention and accumulation of phytoplankton biomass in that area. The presence of a Taylor column [20,21,28,29,36] and persistent negative wind stress curl [49], would also contribute to uplift and retention of deeper, nutrient-rich waters on the shelf, further enhancing chla concentrations between the two islands (Figures 1 and 3).

Current impingement can uplift the thermohaline structure and drive the vertical transport of subsurface nutrient-rich waters on the upstream side of islands [13]. Downstream of islands, turbulent mixing, wake effects, isopycnal shoaling associated with lee eddies, as well as passive advection, can also enhance vertical nutrient exchange and stimulate phytoplankton growth [58,84–86]. Internal waves can also introduce nutrient-rich waters to the surface layers, and in ecosystems where the bathymetric slope is more gradual, internal waves are able to reach shallower waters and stimulate phytoplankton growth in nearshore regions [13,87,110]. The upstream and downstream effects of current impingement, turbulence, isopycnal shoaling, and internal waves on phytoplankton biomass have to date not been examined in detail at the PEIs [26].

Mesoscale eddies can strongly influence the distribution of heat, salt, and phytoplankton biomass through horizontal and vertical exchanges driven by their dynamics and interactions with the surrounding environment [94,111,112]. On the PEI shelf, [28] have shown that mesoscale eddies can cause warming or cooling, ranging between 0.5 and 2 °C. More recently, [35] demonstrated that these eddies interact with the PEI shelf for a substantial portion of the year. Passing mesoscale eddies are thus expected to have a marked effect on the spatial distribution and temporal variations of nutrients and phytoplankton at and around the PEIs [26,32]. Enhanced surface chla has also been associated with mesoscale eddies near the Antarctic Polar Front at the Kerguelen Islands [10]. However, the present study is unable to discern the individual effects of mesoscale eddies on phytoplankton biomass distributions around the islands, since we have used averaged data to present chla climatologies (Figure 3). Given the complex chla patterns that have previously been observed in response to mesoscale eddies in the Southern Ocean, further research is required to better understand the impacts of individual eddies at more local scales around the PEIs.

Despite inherent limitations associated with satellite and reanalysis products, they provide a cost-effective means of examining the spatial distribution and temporal variability of surface hydrography and phytoplankton biomass, particularly in regions such as the PEIs where in situ sampling is severely limited by logistical constraints. While satellite and reanalysis products are useful for examining the spatial extent and temporal variability of elevated chla around isolated island ecosystems such as the PEIs, they provide only surface information. Since both surface and subsurface chla maxima occur in the PEI region [32], it is necessary to improve in situ subsurface observations to better understand the vertical phytoplankton biomass fluctuations. Although the Argo network of profiling floats has significantly improved our ability to measure and understand vertical oceanographic variations in the Southern Ocean, there is still substantial sparsity of such observations in the PEI region, as illustrated by the data gaps evident in Figure S3. Further dedicated and long-term in situ sampling is thus required to improve our understanding of oceanographic variations and their impacts on phytoplankton biomass and ecosystem functioning in this region.

5. Summary and Conclusions

This study presented the first local-scale investigation of the seasonal and spatial variations of chla around the PEIs, enhancing knowledge of the IME associated with the islands. The previously unobserved local-scale chla seasonal cycle illustrated that increases occurred only from October to May, in agreement with the seasonal cycle previously described at other sub-Antarctic islands and in larger scale Southern Ocean studies. The observed spatial patterns suggested, for the first time, the occurrence of both "classical IMEs", where elevated chla is spatially connected to the shelf, as well as "delayed IMEs" where elevated chla becomes separated from the shelf as water masses are advected further away. However, more detailed in situ and/or modelling studies will be required to confirm this hypothesis.

Seasonal chla variations were significantly correlated with seasonal changes in available light, temperature, and upper mixed layer depths. Positive correlations between SST and chla reflected the occurrence of elevated chla during summer and autumn months when surface waters at the PEIs were warmer. Higher chla values were only observed when PAR exceeded 25 E m^{-2} d^{-1} and MLD was shallower than ±80 m, reflecting stronger control of light availability and water column stability on chla, in agreement with other studies in the Southern Ocean. While gridded nutrient data from the WOA 2018 reflected the known large-scale seasonal cycles of nitrate, silicate, and phosphate, the coarse spatial resolution of this data prevented observation of previously described nutrient enhancement on the PEI shelf. In addition, there were no statistically significant relationships between surface nutrients and chla, likely due to the insufficiency of the nutrient observations. This highlights a critical gap in our observations at the PEIs, and it will be essential to improve

the frequency and spatial resolution of nutrient observations if we are to understand the local fluctuations in phytoplankton biomass.

Importantly, while some previous investigations have described chla increases on the small PEI shelf and in association with passing mesoscale eddies, our study showed for the first time that there is a recurrent extension of elevated chla northeast of the island shelf from late spring to early autumn. This previously undocumented region of enhanced chla was clearly associated with weak mean circulation northeast of the islands, suggesting retention and accumulation of nutrients and phytoplankton biomass. Northeastward wind-driven transport likely plays a role in maintaining the advection of nutrients and phytoplankton from the island shelf to this region. With the climatological mean chla in this region being consistently higher than that on the PEI shelf, this area likely provides an important food source and plays a crucial role in supporting the functioning of the rich PEI ecosystem, but further research is needed to adequately discern such effects.

Supplementary Materials: The following supporting information can be downloaded at: https://www.mdpi.com/article/10.3390/rs14092140/s1, Figure S1: (**a**–**l**) Monthly (January to December) Ocean-Colour Climate Change Initiative (OC-CCI) chlorophyll *a* (chla; mg m^{-3}) climatology (1997–2020) in the Prince Edward Island (PEI) region. The dashed brown contour indicates the 1000 m isobath. The solid and dashed thick blue lines show the climatological mean positions of the middle (M-SAF) and southern (S-SAF) branches of the sub-Antarctic Front, respectively. The solid and dotted thick orange lines illustrate the climatological mean positions of the northern (N-APF) and middle (M-APF) branches of the Antarctic Polar Front, respectively. White shading indicates regions where there are no observations during the 1997–2020 period. Figure S2: Temporal variability of the monthly mean Copernicus-Globcolour chlorophyll *a* (chla; 1997–2020), extracted and averaged over the region (45.5–46.5° S; 38–39° E) encompassed by the long-term mean 0.18 mg m^{-3} chla isopleth northeast of the Prince Edward Islands. White shading indicates no observations. Figure S3: (**a**–**l**) Monthly (January to December) climatology (1997–2020) of the Copernicus-Globcolour chlorophyll *a* (chla; mg m^{-3}) over a larger area around the Prince Edward Islands (PEIs). The black box highlights the area around the PEIs illustrated in the main text and in Figure S1. The black contours indicate chla isopleths (0.18 and 0.25 in January, 0.19 and 0.25 in February, 0.20 and 0.25 in March, 0.20 in April, 0.17 in May, 0.15 and 0.16 in October, 0.20 and 0.25 in November, 0.22, 0.25, and 0.29 in December). The dashed brown contour indicates the 1000 m isobath. The dotted, solid, and dashed thick blue lines show the climatological mean positions of the northern (N-SAF), middle (M-SAF), and southern (S-SAF) branches of the sub-Antarctic Front, respectively. The solid, dotted, and dashed thick orange lines illustrate the climatological mean positions of the northern (N-APF), middle (M-APF), and southern (S-APF) branches of the Antarctic Polar Front, respectively. Figure S4: (**a**–**l**) Monthly (January to December) climatology (2000–2019) of the mixed layer depth (m) computed from Argo profiles (Holte et al., 2017) in the Prince Edward Island (PEI) region. The dashed brown contour indicates the 1000 m isobath. White shading indicates regions of no data for the 2000–2019 period. Figure S5: (**a**–**l**) Monthly (January to December) climatology (1993–2019) of the GLORYS2V4 simulated mixed layer depth (m) (Lellouche et al., 2013) in the Prince Edward Island (PEI) region. The dashed brown contour indicates the 1000 m isobath. Figure S6: (**a**–**l**) Monthly (January to December) climatology (1993–2019) of the C-GLORS05 simulated mixed layer depth (m) (Storto et al., 2016) in the Prince Edward Island (PEI) region. The dashed brown contour indicates the 1000 m isobath. Figure S7: (**a**–**l**) Monthly (January to December) climatology (1993–2019) of the GLOSEA5v13 simulated mixed layer depth (m) (MacLachlan et al., 2015) in the Prince Edward Island (PEI) region. The dashed brown contour indicates the 1000 m isobath. Figure S8: (**a**–**l**) Monthly (January to December) World Ocean Atlas 2018 climatology of phosphate (μmol kg^{-1}). The black contours indicate chla (mg m^{-3}) isopleths (0.18 and 0.25 in January, 0.19 and 0.25 in February, 0.20 and 0.25 in March, 0.20 in April, 0.17 in May, 0.15 and 0.16 in October, 0.20 and 0.25 in November, 0.22, 0.25, and 0.29 in December). The dashed brown contours indicate the 1000 m isobath. The solid and dashed thick blue lines show the climatological mean positions of the middle (M-SAF) and southern (S-SAF) branches of the sub-Antarctic Front, respectively. The solid and dotted thick orange lines illustrate the climatological mean positions of the northern (N-APF) and middle (M-APF) branches of the Antarctic Polar Front, respectively. Figure S9: Pearson correlation between monthly chlorophyll *a* (chla) and (**a**) wind speed, (**b**) wind stress curl, (**c**) geostrophic current speed, and (**d**) Ekman current speed. The dashed brown contours

show the 1000 m isobath. The black contours illustrate the long-term mean 0.18 mg m^{-3} chla isopleths. The solid and dashed thick blue lines show the long-term mean positions of the middle (M-SAF) and southern (S-SAF) branches of the sub-Antarctic Front, respectively. The solid and dotted thick orange lines illustrate the long-term mean positions of the northern (N-APF) and middle (M-APF) branches of the Antarctic Polar Front, respectively.

Author Contributions: Conceptualization, T.L.; methodology, T.L.; software, T.L. and T.T.; validation, T.L. and T.T.; formal analysis, T.L. and T.T.; investigation, T.L. and T.T.; resources, T.L.; data curation, T.L. and T.T.; writing—original draft preparation, T.L. and T.T.; writing—review and editing, T.L. and T.T.; visualization, T.T.; supervision, T.L.; project administration, T.L.; funding acquisition, T.L. All authors have read and agreed to the published version of the manuscript.

Funding: This research was funded by the Oceans & Coasts Research Branch of the South African Department of Forestry, Fisheries, and the Environment (DFFE), the Bayworld Centre for Research and Education (BCRE), and the South African National Research Foundation (NRF grant: 129229).

Data Availability Statement: The Copernicus GlobColour satellite chla, sea surface temperature, altimetry, and Global Ocean Ensemble Reanalysis Mixed Layer Depth (MLD), are produced and distributed by the Copernicus Marine Environment Monitoring Service (CMEMS, https://marine.copernicus.eu/, accessed on 25 August 2021). Modelled Ekman current were obtained from IFREMER (http://globcurrent.ifremer.fr, accessed on 20 January 2021). ERA5 wind products are provided by the European Center for Medium-Range Weather Forecasts (ECMWF; https://cds.climate.copernicus.eu/#!/search?text=ERA5&type=dataset, accessed on 20 January 2021). The Argo MLD climatology is available at http://mixedlayer.ucsd.edu/ (accessed on 25 August 2021), and monthly nutrient climatologies were obtained from the World Ocean Atlas 2018 (https://www.ncei.noaa.gov/data/oceans/woa/WOA18/DATA/, accessed on 28 August 2021). SeaWiFS and MODIS Aqua Photosynthetically Available Radiation was obtained from the Ocean Biology Processing Group at the Ocean Ecology Laboratory, NASA Goddard Space Flight Center (https://oceandata.sci.gsfc.nasa.gov/directaccess/, accessed on 25 August 2021).

Acknowledgments: We are grateful to the Oceans & Coasts Research Branch of the South African Department of Forestry, Fisheries, and the Environment (DFFE), the Bayworld Centre for Research and Education (BCRE), as well as the South African National Research Foundation (NRF grant: 129229) for funding support, and administrative and logistical assistance.

Conflicts of Interest: The authors declare no conflict of interest. The funding agencies had no role in the design of the study; in the collection, analysis, or interpretation of data; in the writing of the manuscript, and in the decision to publish the results.

References

1. Deppeler, S.L.; Davidson, A.T. Southern Ocean phytoplankton in a changing climate. *Front. Mar. Sci.* **2017**, *4*, 40. [CrossRef]
2. Pinkerton, M.H.; Boyd, P.W.; Deppeler, S.; Hayward, A.; Höfer, J.; Moreau, S. Evidence for the impact of climate change on primary producers in the Southern Ocean. *Front. Ecol. Evol.* **2021**, *9*, 592027. [CrossRef]
3. Rogers, A.D.; Frinault, B.A.V.; Barnes, D.K.A.; Bindoff, N.L.; Downie, R.; Ducklow, H.W.; Friedlaender, A.S.; Hart, T.; Hill, S.L.; Hofmann, E.E.; et al. Antarctic Futures: An assessment of climate-driven changes in ecosystem structure, function, and service provisioning in the Southern Ocean. *Ann. Rev. Mar. Sci.* **2020**, *12*, 87–120. [CrossRef] [PubMed]
4. Sarmiento, J.L.; Gruber, N.; Brzezinski, M.A.; Dunne, J.P. High-latitude controls of thermocline nutrients and low latitude biological productivity. *Nature* **2004**, *427*, 56–60. [CrossRef] [PubMed]
5. Arrigo, K.R.; van Dijken, G.L.; Bushinsky, S. Primary production in the Southern Ocean, 1997–2006. *J. Geophys. Res.* **2008**, *113*, C08004. [CrossRef]
6. Bristow, L.A.; Mohr, W.; Ahmerkamp, S.; Kuypers, M.M.M. Nutrients that limit growth in the ocean. *Curr. Biol.* **2017**, *27*, R431–R510. [CrossRef] [PubMed]
7. Venables, H.; Moore, C.M. Phytoplankton and light limitation in the Southern Ocean: Learning from high-nutrient, high-chlorophyll areas. *J. Geophys. Res.* **2010**, *115*, C02015. [CrossRef]
8. Browning, T.J.; Achterberg, E.P.; Engel, A.; Mawji, E. Manganese co-limitation of phytoplankton growth and major nutrient drawdown in the Southern Ocean. *Nat. Commun.* **2021**, *12*, 884. [CrossRef]
9. Graham, R.M.; De Boer, A.M.; van Sebille, E.; Kohfeld, K.E.; Schlosser, C. Inferring source regions and supply mechanisms of iron in the Southern Ocean from satellite chlorophyll data. *Deep-Sea Res. I* **2005**, *104*, 9–25. [CrossRef]
10. Moore, J.K.; Abbott, M.R. Surface chlorophyll concentrations in relation to the Antarctic Polar Front: Seasonal and spatial patterns from satellite observations. *J. Mar. Syst.* **2002**, *37*, 69–86. [CrossRef]

11. Sokolov, S.; Rintoul, S.R. On the relationship between fronts and the Antarctic Circumpolar Current and surface chlorophyll concentrations in the Southern Ocean. *J. Geophys. Res.* **2007**, *112*, C07030. [CrossRef]
12. Boden, B.P. Observations of the island mass effect in the Prince Edward archipelago. *Polar Biol.* **1988**, *9*, 61–68. [CrossRef]
13. Gove, J.M.; McManus, M.A.; Neuheimer, A.B.; Polovina, J.J.; Drazen, J.C.; Smith, C.R.; Merrifield, M.A.; Friedlander, A.M.; Ehses, J.S.; Young, C.W.; et al. Near-island biological hotspots in barren ocean basins. *Nat. Commun.* **2016**, *7*, 10581. [CrossRef] [PubMed]
14. Gove, J.M.; Williams, G.J.; McManus, M.A.; Heron, S.F.; Sandin, S.A.; Vetter, O.J.; Foley, D.G. Quantifying climatological ranges and anomalies for Pacific coral reef ecosystems. *PLoS ONE* **2013**, *8*, e61974. [CrossRef] [PubMed]
15. Jones, E.M.; Bakker, D.C.E.; Venables, H.J.; Watson, A.J. Dynamic seasonal cycling of inorganic carbon downstream of South Georgia, Southern Ocean. *Deep-Sea Res. II* **2012**, *59–60*, 25–35. [CrossRef]
16. Quilty, P.G. Origin and evolution of the sub-Antarctic islands: The foundation. *Pap. Proc. R. Soc. Tasmania* **2007**, *141*, 35–58. [CrossRef]
17. Lutjeharms, J.R.E.; Ansorge, I.J. Oceanographic setting of the Prince Edward Islands. In *The Prince Edward Islands: Land-Sea Interactions in a Changing Ecosystem*; Chown, S.L., Froneman, P.W., Eds.; Sun Press: Stellenbosch, South Africa, 2008; pp. 17–38.
18. Whitehead, O.; von der Meden, C.; Skowno, A.L.; Sink, K.J.; van der Merwe, S.; Adams, R.; Holness, S. (Eds.) *South African National Biodiversity Assessment 2018 Technical Report Volume 6: Sub-Antarctic Territory*; South African National Biodiversity Institute: Pretoria, South Africa, 2019; Available online: http://hdl.handle.net/20.500.12143/6375 (accessed on 20 September 2021).
19. Kirkman, S.P.; Yemane, D.G.; Lamont, T.; Meÿer, M.A.; Pistorius, P.A. Foraging behaviour of Subantarctic Fur Seals supports efficiency of a marine reserve's design. *PLoS ONE* **2016**, *11*, e0152370. [CrossRef]
20. Pakhomov, E.A.; Froneman, P.W. The Prince Edward Islands pelagic ecosystem: A review of achievements 1976–1990. *J. Mar. Syst.* **1999**, *18*, 297–310. [CrossRef]
21. Pakhomov, E.A.; Froneman, P.W. Macroplankton/micronekton dynamics in the vicinity of the Prince Edward Islands (Southern Ocean). *Mar. Biol.* **1999**, *134*, 501–515. [CrossRef]
22. Perissinotto, R.; McQuaid, C.D. Land-based predator impact on vertically migrating zooplankton and micronekton advected to a Southern Ocean archipelago. *Mar. Ecol. Prog. Ser.* **1992**, *80*, 15–27. [CrossRef]
23. Ryan, P.G.; Bester, M.N. Pelagic predators. In *The Prince Edward Islands: Land-Sea Interactions in a Changing Ecosystem*; Chown, S.L., Froneman, P.W., Eds.; Sun Press: Stellenbosch, South Africa, 2008; pp. 121–164.
24. von der Meden, C.E.O.; Atkinson, L.J.; Branch, G.M.; Asdar, S.; Ansorge, I.J.; van den Berg, M. Long-term change in epibenthic assemblages at the Prince Edward Islands: A comparison between 1988 and 2013. *Polar Biol.* **2017**, *40*, 2171–2185. [CrossRef]
25. Pakhomov, E.A.; Chown, S.L. The Prince Edward Islands: Southern Ocean Oasis. *Ocean Yearb.* **2003**, *17*, 348–379. [CrossRef]
26. McQuaid, C.D.; Froneman, P.W. Biology in the oceanographic environment. In *The Prince Edward Islands: Land-Sea Interactions in a Changing Ecosystem*; Chown, S.L., Froneman, P.W., Eds.; Sun Press: Stellenbosch, South Africa, 2008; pp. 97–120.
27. Rae, C.M.D. Physical and chemical marine environment of the Prince Edward Islands (Southern Ocean) during April/May 1987. *S. Afr. J. Mar. Sci.* **1989**, *8*, 301–311. [CrossRef]
28. Lamont, T.; van den Berg, M.A.; Tutt, G.C.O.; Ansorge, I.J. Impact of deep-ocean eddies and fronts on the shelf seas of a sub-Antarctic Archipelago: The Prince Edward Islands. *Cont. Shelf Res.* **2019**, *177*, 1–14. [CrossRef]
29. Perissinotto, R.; Duncombe Rae, C.M. Occurrence of anti-cyclonic eddies on the Prince Edward Plateau (Southern Ocean): Effects on phytoplankton biomass and production. *Deep-Sea Res. I* **1990**, *37*, 777–793. [CrossRef]
30. Perissinotto, R.; Duncombe Rae, C.M.; Boden, B.P.; Allanson, B.R. Vertical stability as a controlling factor of the marine phytoplankton production at the Prince Edward Archipelago (Southern Ocean). *Mar. Ecol. Prog. Ser.* **1990**, *60*, 205–209. [CrossRef]
31. Pakhomov, E.A.; Froneman, P.W.; Ansorge, I.J.; Lutjeharms, J.R.E. Temporal variability in the physico-biological environment of the Prince Edward Islands (Southern Ocean). *J. Mar. Syst.* **2000**, *26*, 75–95. [CrossRef]
32. Lamont, T.; Tutt, G.C.O.; Barlow, R.G. Phytoplankton biomass and photophysiology at the sub-Antarctic Prince Edward Islands ecosystem in the Southern Ocean. *J. Mar. Syst.* **2022**, *226*, 103669. [CrossRef]
33. Bernard, A.T.F.; Ansorge, I.J.; Froneman, P.W.; Lutjeharms, J.R.E.; Bernard, K.S.; Swart, N.C. Entrainment of Antarctic euphausiids across the Antarctic Polar Front by a cold eddy. *Deep-Sea Res. I* **2007**, *54*, 1841–1851. [CrossRef]
34. Pakhomov, E.A.; Ansorge, I.J.; Froneman, P.W. Variability in the inter-island environment of the Prince Edward Islands (Southern Ocean). *Polar Biol.* **2000**, *23*, 593–603. [CrossRef]
35. Lamont, T.; van den Berg, M.A. Mesoscale eddies influencing the sub-Antarctic Prince Edward Islands Archipelago: Temporal variability and impact. *Cont. Shelf Res.* **2021**, *212*, 104309. [CrossRef]
36. Perissinotto, R.; Lutjeharms, J.R.E.; van Ballegooyen, R.C. Biological-physical interactions and pelagic productivity at the Prince Edward Islands, Southern Ocean. *J. Mar. Syst.* **2000**, *24*, 327–341. [CrossRef]
37. Ansorge, I.J.; Lutjeharms, J.R.E. Eddies originating at the South-West Indian Ridge. *J. Mar. Syst.* **2003**, *39*, 1–18. [CrossRef]
38. Ansorge, I.J.; Lutjeharms, J.R.E. Direct observations of eddy turbulence at a ridge in the Southern Ocean. *Geophys. Res. Lett.* **2005**, *32*, L14603. [CrossRef]
39. Durgadoo, J.V.; Ansorge, I.J.; de Cuevas, B.A.; Lutjeharms, J.R.E.; Coward, A.C. Decay of eddies at the South-West Indian Ridge. *S. Afr. J. Sci.* **2011**, *107*, 673. [CrossRef]
40. Durgadoo, J.V.; Ansorge, I.J.; Lutjeharms, J.R.E. Oceanographic observations of eddies impacting the Prince Edward Islands, South Africa. *Antarct. Sci.* **2010**, *22*, 211–219. [CrossRef]

41. Lamont, T.; van den Berg, M.A. Mesoscale eddies influencing the sub-Antarctic Prince Edward Islands Archipelago: Origin, Pathways, and Characteristics. *Cont. Shelf Res.* **2020**, *210*, 104257. [CrossRef]
42. Ansorge, I.J.; Froneman, P.W.; Pakhomov, E.A.; Lutjeharms, J.R.E.; Perissinotto, R.; van Ballegooyen, R.C. Physical-biological coupling in the waters surrounding the Prince Edward Islands (Southern Ocean). *Polar Biol.* **1999**, *21*, 135–145. [CrossRef]
43. Ansorge, I.J.; Durgadoo, J.V.; Pakhomov, E.A. Dynamics of physical and biological systems of the Prince Edward Islands in a changing climate. *Pap. Proc. R. Soc. Tasmania* **2009**, *143*, 15–18. [CrossRef]
44. Ansorge, I.J.; Froneman, P.W.; Durgadoo, J.V. The marine ecosystem of the sub-Antarctic, Prince Edward Islands. In *Marine Ecosystems*; Cruzado, A., Ed.; InTech Press: Rijeka, Croatia, 2011; pp. 61–76. [CrossRef]
45. Ansorge, I.J.; Lutjeharms, J.R.E. The hydrography and dynamics of the ocean environment of the Prince Edward Islands (Southern Ocean). *J. Mar. Syst.* **2002**, *37*, 107–127. [CrossRef]
46. Stirnimann, L.; Bornman, T.G.; Verheye, H.M.; Bachèlery, M.-L.; van der Poel, J.; Fawcett, S.E. Plankton community composition and productivity near the Subantarctic Prince Edward Islands archipelago in autumn. *Limnol. Oceanogr.* **2021**, *66*, 4140–4158. [CrossRef]
47. Venkatachalam, S.; Matcher, G.F.; Lamont, T.; van den Berg, M.; Ansorge, I.J.; Dorrington, R.A. Influence of oceanographic variability on near-shore microbial communities of the sub-Antarctic Prince Edward Islands. *Limnol. Oceanogr.* **2019**, *64*, 258–271. [CrossRef]
48. Chown, S.L.; Froneman, P.W. (Eds.) *The Prince Edward Islands: Land-Sea Interactions in a Changing Ecosystem*; Sun Press: Stellenbosch, South Africa, 2008. [CrossRef]
49. Toolsee, T.; Lamont, T.; Rouault, M.; Ansorge, I. Characterising the seasonal cycle of wind forcing, surface circulation and temperature around the sub-Antarctic Prince Edward Islands. *Afr. J. Mar. Sci.* **2021**, *43*, 61–76. [CrossRef]
50. Ardyna, M.; Clautre, H.; Sallée, J.-B.; d'Ovidio, F.; Gentili, B.; van Dijken, G.; D'Ortenzio, F.; Arrigo, K.R. Delineating environmental control of phytoplankton biomass and phenology in the Southern Ocean. *Geophys. Res. Lett.* **2017**, *44*, 5016–5024. [CrossRef]
51. Lamont, T.; Brewin, R.J.W.; Barlow, R.G. Seasonal variation in remotely-sensed phytoplankton size structure around southern Africa. *Remote Sens. Environ.* **2018**, *204*, 617–631. [CrossRef]
52. Mongin, M.; Molina, E.; Trull, T.W. Seasonality and scale of the Kergeulen plateau phytoplankton bloom: A remote sensing and modelling analysis of the influence of natural iron fertilization in the Southern Ocean. *Deep-Sea Res. II* **2008**, *55*, 880–892. [CrossRef]
53. Thomalla, S.J.; Fauchereau, N.; Swart, S.; Monteiro, P.M.S. Regional scale characteristics of the seasonal cycle of chlorophyll in the Southern Ocean. *Biogeosciences* **2011**, *8*, 2849–2866. [CrossRef]
54. Del Castillo, C.E.; Signorini, S.R.; Karaköylü, E.M.; Rivero-Calle, S. Is the Southern Ocean getting greener? *Geophys. Res. Lett.* **2019**, *46*, 6034–6040. [CrossRef] [PubMed]
55. Kahru, M.; Mitchell, B.G. Blending of ocean colour algorithms applied to the Southern Ocean. *Remote Sens. Lett.* **2010**, *1*, 119–124. [CrossRef]
56. Garnesson, P.; Mangin, A.; Fanton d'Andon, O.; Demaria, J.; Bretagnon, M. The CMEMS GlobColour chlorophyll a product based on satellite observation: Multi-sensor merging and flagging strategies. *Ocean Sci.* **2019**, *15*, 819–830. [CrossRef]
57. Sathyendranath, S.; Brewin, R.J.W.; Brockmann, C.; Brotas, V.; Calton, B.; Chuprin, A.; Cipollini, P.; Couto, A.B.; Dingle, J.; Doerffer, R.; et al. An Ocean-Colour time series for use in climate studies: The experience of the Ocean-Colour Climate Change Initiative (OC-CCI). *Sensors* **2019**, *19*, 4285. [CrossRef] [PubMed]
58. Shiozaki, T.; Kodama, T.; Furuya, K. Large-scale impact of the island mass effect through nitrogen fixation in the western South Pacific Ocean. *Geophys. Res. Lett.* **2014**, *41*, 2907–2913. [CrossRef]
59. Jena, B. Satellite remote sensing of the island mass effect on the Sub-Antarctic Kerguelen Plateau, Southern Ocean. *Front. Earth Sci.* **2016**, *10*, 479–486. [CrossRef]
60. Martinez, E.; Maamaatuaiahutapu, K. Island mass effect in the Marquesas Islands: Time variation. *Geophys. Res. Lett.* **2004**, *31*, L18307. [CrossRef]
61. NASA Goddard Space Flight Center, Ocean Ecology Laboratory, Ocean Biology Processing Group. *Sea-Viewing Wide Field-of-View Sensor (SeaWiFS) Photosynthetically Available Radiation Data*; 2018 Reprocessing; NASA OB.DAAC: Greenbelt, MD, USA, 2018. Available online: https://oceancolor.gsfc.nasa.gov/data/10.5067/ORBVIEW-2/SEAWIFS/L3M/PAR/2018/ (accessed on 25 August 2021).
62. NASA Goddard Space Flight Center, Ocean Ecology Laboratory, Ocean Biology Processing Group. *Moderate-Resolution Imaging Spectroradiometer (MODIS) Aqua Photosynthetically Available Radiation Data*; 2018 Reprocessing; NASA OB.DAAC: Greenbelt, MD, USA, 2018. [CrossRef]
63. Garcia, H.E.; Weathers, K.W.; Paver, C.R.; Smolyar, I.; Boyer, T.P.; Locarnini, R.A.; Zweng, M.M.; Mishonov, A.V.; Baranova, O.K.; Seidov, D.; et al. *World Ocean Atlas 2018. Vol. 4: Dissolved Inorganic Nutrients (Phosphate, Nitrate and Nitrate + Nitrite, Silicate)*; Mishonov, A., Ed.; NOAA Atlas NESDIS: Silver Spring, MD, USA, 2019; Volume 84, 35p.
64. Taburet, G.; Sanchez-Roman, A.; Ballarotta, M.; Pujol, M.-I.; Legeais, J.-F.; Fournier, F.; Faugere, Y.; Dibarbourne, G. DUACS DT2018: 25 years of reprocessed sea level altimetry records. *Ocean Sci.* **2019**, *15*, 1207–1224. [CrossRef]
65. Rio, M.-H.; Mulet, S.; Picot, N. Beyond GOCE for the ocean circulation estimate: Synergetic use of altimetry, gravimetry, and in situ data provides new insight into geostrophic and Ekman currents. *Geophys. Res. Lett.* **2014**, *41*, 8919–8925. [CrossRef]

66. Sokolov, S.; Rintoul, S.R. Circumpolar structure and distribution of the Antarctic Circumpolar Current fronts: 1. Mean circumpolar paths. *J. Geophys. Res.* **2009**, *114*, C11018. [CrossRef]
67. Sokolov, S.; Rintoul, S.R. Circumpolar structure and distribution of the Antarctic Circumpolar Current fronts: 2. Variability and relationship to sea surface height. *J. Geophys. Res.* **2009**, *114*, C11019. [CrossRef]
68. Good, S.; Fiedler, E.; Mao, C.; Martin, M.J.; Maycock, A.; Reid, R.; Roberts-Jones, J.; Searle, T.; Waters, J.; While, J.; et al. The current configuration of the OSTIA system for operational production of foundation sea surface temperature and ice concentration analyses. *Remote Sens.* **2020**, *12*, 720. [CrossRef]
69. Hersbach, H.; Bell, B.; Berrisford, P.; Biavati, G.; Horányi, A.; Muñoz Sabater, J.; Nicolas, J.; Peubey, C.; Radu, R.; Rozum, I.; et al. ERA5 hourly Data on Pressure Levels from 1979 to Present. Copernicus Climate Change Service (C3S) Climate Data Store (CDS). 2018. Available online: https://cds.climate.copernicus.eu/cdsapp#!/dataset/10.24381/cds.bd0915c6?tab=overview (accessed on 20 January 2021).
70. Trenberth, K.E.; Large, W.G.; Olson, J.G. The mean annual cycle in global ocean wind stress. *J. Phys. Oceanogr.* **1990**, *20*, 1742–1760. [CrossRef]
71. Risien, C.M.; Chelton, D.B. A global climatology of surface wind and wind stress fields from eight years of QuikSCAT scatterometer data. *J. Phys. Oceanogr.* **2008**, *38*, 2379–2413. [CrossRef]
72. Holte, J.; Talley, L.D.; Gilson, J.; Roemmich, D. An Argo mixed layer climatology and database. *Geophys. Res. Lett.* **2017**, *44*, 5618–5626. [CrossRef]
73. Zuo, H.; Balmaseda, M.A.; Tietsche, S.; Mogensen, K.; Mayer, M. The ECMWF operational ensemble reanalysis–analysis system for ocean and sea ice: A description of the system and assessment. *Ocean Sci.* **2019**, *15*, 779–808. [CrossRef]
74. Lellouche, J.-M.; Le Galloudec, O.; Drévillon, M.; Régnier, C.; Greiner, E.; Garric, G.; Ferry, N.; Desportes, C.; Testut, C.-E.; Bricaud, C.; et al. Evaluation of global monitoring and forecasting systems at Mercator Océan. *Ocean Sci.* **2013**, *9*, 57–81. [CrossRef]
75. Storto, A.; Masina, S.; Navarra, A. Evaluation of the CMCC eddy-permitting global ocean physical reanalysis system (C-GLORS, 1982-2012) and its assimilation components. *Q. J. R. Meteorol. Soc.* **2016**, *142*, 738–758. [CrossRef]
76. MacLachlan, C.; Arribas, A.; Peterson, K.A.; Maidens, A.; Fereday, D.; Scaife, A.A.; Gordon, M.; Vellinga, M.; Williams, A.; Comer, R.E.; et al. Global seasonal forecast system version 5 (GloSea5): A high-resolution seasonal forecast system. *Q. J. R. Meteorol. Soc.* **2015**, *141*, 1072–1084. [CrossRef]
77. Korb, R.E.; Whitehouse, M.J.; Atkinson, A.; Thorpe, S.E. Magnitude and maintenance of the phytoplankton bloom at South Georgia: A naturally iron-replete environment. *Mar. Ecol. Prog. Ser.* **2008**, *368*, 75–91. [CrossRef]
78. Venables, H.J.; Pollard, R.T.; Popova, E.E. Physical conditions controlling the development of a regular phytoplankton bloom north of the Crozet Plateau, Southern Ocean. *Deep-Sea Res. II* **2007**, *54*, 1949–1965. [CrossRef]
79. Rouault, M.; Mélice, J.-L.; Reason, C.J.C.; Lutjeharms, J.R.E. Climate variability at Marion Island, Southern Ocean, since 1960. *J. Geophys. Res.* **2005**, *110*, C05007. [CrossRef]
80. Rintoul, S.R. The global influence of localized dynamics in the Southern Ocean. *Nature* **2018**, *558*, 209–218. [CrossRef] [PubMed]
81. Atkinson, A.; Whitehouse, M.J.; Priddle, J.; Cripps, G.C.; Ward, P.; Brandon, M.A. South Georgia, Antarctica: A productive, cold water, pelagic ecosystem. *Mar. Ecol. Prog. Ser.* **2001**, *216*, 279–308. [CrossRef]
82. Korb, R.E.; Whitehouse, M.J.; Ward, P. SeaWiFS in the Southern Ocean: Spatial and temporal variability in phytoplankton biomass around South Georgia. *Deep-Sea Res. II* **2004**, *51*, 99–116. [CrossRef]
83. Moore, J.K.; Abbott, M.R. Phytoplankton chlorophyll distributions and primary production in the Southern Ocean. *J. Geophys. Res.* **2000**, *105*, 28709–28722. [CrossRef]
84. Hasegawa, D.; Yamazaki, H.; Ishimaru, T.; Nagashima, H.; Koike, Y. Apparent phytoplankton bloom due to island mass effect. *J. Mar. Syst.* **2008**, *69*, 238–246. [CrossRef]
85. Hasegawa, D.; Lewis, M.R.; Gangopadhyay, A. How islands cause phytoplankton to bloom in their wakes. *Geophys. Res. Lett.* **2009**, *36*, L20605. [CrossRef]
86. Messié, M.; Petrenko, A.; Doglioli, A.M.; Aldebert, C.; Martinez, E.; Koenig, G.; Bonnet, S.; Moutin, T. The delayed Island Mass Effect: How islands can remotely trigger blooms in the oligotrophic ocean. *Geophys. Res. Lett.* **2020**, *47*, e2019GL085282. [CrossRef]
87. Blain, S.; Quéguiner, B.; Armand, L.; Belviso, S.; Bombled, B.; Bopp, L.; Bowie, A.; Brunet, C.; Brussard, C.; Carlottie, F.; et al. Effect of natural iron fertilization on carbon sequestration in the Southern Ocean. *Nature* **2007**, *446*, 7139. [CrossRef] [PubMed]
88. Swart, S.; Thomalla, S.J.; Monteiro, P.M.S. The seasonal cycle of mixed layer dynamics and phytoplankton biomass in the Sub-Antarctic Zone: A high-resolution glider experiment. *J. Mar. Syst.* **2015**, *147*, 103–115. [CrossRef]
89. Arteaga, L.A.; Boss, E.; Behrenfeld, M.J.; Westberry, T.K.; Sarmiento, J.L. Seasonal modulation of phytoplankton biomass in the Southern Ocean. *Nat. Commun.* **2020**, *11*, 5364. [CrossRef] [PubMed]
90. Ratnarajah, L.; Blain, S.; Boyd, P.W.; Fourquez, M.; Obernosterer, I.; Tagliabue, A. Resource colimitation drives competition between phytoplankton and bacteria in the Southern Ocean. *Geophys. Res. Lett.* **2021**, *48*, e2020GL088369. [CrossRef] [PubMed]
91. Behrenfeld, M.J.; O'Malley, R.T.; Siegel, D.A.; McClain, C.R.; Sarmiento, J.L.; Feldman, G.C.; Milligan, A.J.; Falkowski, P.G.; Letelier, R.M.; Boss, E.S. Climate-driven trends in contemporary ocean productivity. *Nature* **2006**, *444*, 752–755. [CrossRef] [PubMed]
92. Boyce, D.G.; Lewis, M.R.; Worm, B. Global phytoplankton decline over the past century. *Nature* **2010**, *466*, 591–596. [CrossRef] [PubMed]

93. Gregg, W.W.; Casey, N.W.; McClain, C.R. Recent trends in global ocean chlorophyll. *Geophys. Res. Lett.* **2005**, *32*, L03606. [CrossRef]
94. Zhao, D.; Gao, L.; Xu, Y. Quantification of the impact of environmental factors on chlorophyll in the open ocean. *J. Oceanol. Limnol.* **2021**, *39*, 447–457. [CrossRef]
95. Dunstan, P.K.; Foster, S.D.; King, E.; Risbey, J.; O'Kane, T.J.; Monselesan, D.; Hobday, A.J.; Hartog, J.R.; Thompson, P.A. Global patterns of change and variation in sea surface temperature and chlorophyll a. *Sci. Rep.* **2018**, *8*, 14624. [CrossRef]
96. Feng, J.; Durant, J.M.; Stige, L.C.; Hessen, D.O.; Hjermann, D.Ø.; Zhu, L.; Llope, M.; Stenseth, N.C. Contrasting correlation patterns between environmental factors and chlorophyll levels in the global ocean. *Global Biogeochem. Cycles* **2015**, *29*, 2095–2107. [CrossRef]
97. Sarmiento, J.L.; Slater, R.; Barber, R.; Bopp, L.; Doney, S.C.; Hirst, A.C.; Kleypas, J.; Matear, R.; Mikolajewicz, U.; Monfray, P.; et al. Response of ocean ecosystems to climate warming. *Global Biogeochem. Cycles* **2004**, *18*, GB3003. [CrossRef]
98. Boyd, P.W.; Dilllingham, P.W.; McGraw, C.M.; Armstrong, E.A.; Cornwall, C.E.; Feng, Y.-Y.; Hurd, C.L.; Gault-Ringold, M.; Roleda, M.Y.; Timmins-Schiffman, E.; et al. Physiological responses of a Southern Ocean diatom to complex future ocean conditions. *Nat. Clim. Chang.* **2016**, *6*, 207–213. [CrossRef]
99. Montie, S.; Thomsen, M.S.; Rack, W.; Broady, P.A. Extreme summer marine heatwaves increase chlorophyll a in the Southern Ocean. *Antarct. Sci.* **2020**, *32*, 508–509. [CrossRef]
100. Smith, V.R.; Froneman, P.W. 2008. Nutrient dynamics in the vicinity of the Prince Edward Islands. In *The Prince Edward Islands: Land-Sea Interactions in a Changing Ecosystem*; Chown, S.L., Froneman, P.W., Eds.; Sun Press: Stellenbosch, South Africa, 2008; pp. 165–179.
101. Closset, I.; Lasbleiz, M.; Leblanc, K.; Quéguiner, B.; Cavanga, A.-J.; Elskens, M.; Navez, J.; Cardinal, D. Seasonal evolution of net and regenerated silica production around a natural Fe-fertilized area in the Southern Ocean estimated with Si isotopic approaches. *Biogeosciences* **2014**, *11*, 5827–5846. [CrossRef]
102. Pollard, R.T.; Venables, H.J.; Read, J.F.; Allen, J.T. Large-scale circulation around the Crozet Plateau controls an annual phytoplankton bloom in the Crozet Basin. *Deep-Sea Res. II* **2007**, *54*, 1915–1929. [CrossRef]
103. Puccinelli, E.; Smart, S.M.; Fawcett, S.E. Temporal variability in the trophic composition of benthic invertebrates in the Indian sub-Antarctic Ocean. *Deep-Sea Res. I* **2020**, *163*, 103340. [CrossRef]
104. Fourquez, M.; Bressac, M.; Deppeler, S.L.; Ellwood, M.; Obernosterer, I.; Trull, T.W.; Boyd, P.W. Microbial competition in the subpolar Southern Ocean: An Fe-C co-limitation experiment. *Front. Mar. Sci.* **2020**, *6*, 776. [CrossRef]
105. Planquette, H.; Statham, P.J.; Fones, G.R.; Charette, M.A.; Moore, C.M.; Salter, I.; Nédélec, F.H.; Taylor, S.L.; French, M.; Baker, A.R.; et al. Dissolved iron in the vicinity of the Crozet Islands, Southern Ocean. *Deep-Sea Res. II* **2007**, *54*, 1999–2019. [CrossRef]
106. Carranza, M.M.; Gille, S.T. Southern Ocean wind-driven entrainment enhances satellite chlorophyll-a through the summer. *J. Geophys. Res. Oceans* **2015**, *120*, 304–323. [CrossRef]
107. Kahru, M.; Gille, S.T.; Murtugudde, R.; Strutton, P.G.; Manzano-Sarabia, M.; Wang, H.; Mitchell, B.G. Global correlations between winds and ocean chlorophyll. *J. Geophys. Res.* **2010**, *115*, C12040. [CrossRef]
108. Pellichero, V.; Boutin, J.; Claustre, H.; Merlivat, L.; Sallée, J.-B.; Blain, S. Relaxation of wind stress drives the abrupt onset of biological carbon uptake in the Kergeulen bloom: A multisensory approach. *Geophys. Res. Lett.* **2020**, *47*, e2019GL085992. [CrossRef]
109. Irion, S.; Jardillier, L.; Sassenhagen, I.; Christaki, U. Marked spatiotemporal variations in small phytoplankton structure in contrasted waters of the Southern Ocean (Kerguelen area). *Limnol. Oceanogr.* **2020**, *65*, 2835–2852. [CrossRef]
110. Nikurashin, M.; Ferrari, R. Overturning circulation driven by breaking internal waves in the deep ocean. *Geophys. Res. Lett.* **2013**, *40*, 3133–3137. [CrossRef]
111. Dawson, H.R.S.; Strutton, P.G.; Gaube, P. The unusual surface chlorophyll signatures of Southern Ocean eddies. *J. Geophys. Res. Oceans* **2018**, *123*, 6053–6069. [CrossRef]
112. Frenger, I.; Münnich, M.; Gruber, N. Imprint of Southern Ocean mesoscale eddies on chlorophyll. *Biogeosciences* **2018**, *15*, 4781–4798. [CrossRef]